Publication I

E. Nieppola, M. Tornikoski, and E. Valtaoja. 2006. Spectral energy distributions of a large sample of BL Lacertae objects. Astronomy & Astrophysics, volume 445, number 2, pages 441-450.

A&A 445, 441–450 (2006)
DOI: 10.1051/0004-6361:20053316

Astronomy & Astrophysics

Spectral energy distributions of a large sample of BL Lacertae objects⋆

E. Nieppola[1], M. Tornikoski[2], and E. Valtaoja[1,3]

[1] Tuorla Observatory, Väisäläntie 20, 21500 Piikkiö, Finland
e-mail: eni@kurp.hut.fi
[2] Metsähovi Radio Observatory, Metsähovintie 114, 02540 Kylmälä, Finland
[3] Dept. of Physical Sciences, University of Turku, 20100 Turku, Finland

Received 26 April 2005 / Accepted 26 August 2005

ABSTRACT

We have collected a large amount of multifrequency data for objects in the Metsähovi Radio Observatory BL Lacertae sample and computed their spectral energy distributions (SED) in the $\log \nu$ – $\log\ \nu F$ – representation. This is the first time the SEDs of BL Lacs have been studied with a sample of over 300 objects. The synchrotron components of the SEDs were fitted with a parabolic function to determine the synchrotron peak frequency, $\nu_{\rm peak}$. We checked the dependence between luminosities at several frequency bands and synchrotron peak frequency to test the blazar sequence scenario, which states that the source luminosity depends on the location of the synchrotron peak. We also calculated broad band spectral indices and plotted them against each other and $\nu_{\rm peak}$.

The range of $\nu_{\rm peak}$ in our study was considerably extended compared to previous studies. There were 22 objects for which $\log \nu_{\rm peak} > 19$. The data shows that at 5 GHz, 37 GHz, and 5500 Å, there is negative correlation between luminosity and $\nu_{\rm peak}$, whereas in X-rays the correlation turns slightly positive. There is no significant correlation between source luminosity at synchrotron peak and $\nu_{\rm peak}$. Several low radio luminosity-low energy peaked BL Lacs were found. The negative correlation between broad band spectral indices and $\nu_{\rm peak}$ is also significant, although there is substantial scatter. Therefore we find that neither $\alpha_{\rm rx}$ nor $\alpha_{\rm ro}$ can be used to determine the synchrotron peak of BL Lacs. On the grounds of our results, we conclude that the blazar sequence scenario is not valid. In all our results, the BL Lac population is continuous with no hint of the bimodality of the first BL Lac samples.

Key words. galaxies: active – BL Lacertae objects: general – radiation mechanisms: non-thermal

1. Introduction

BL Lacertae (BL Lacs) are a subclass of active galactic nuclei (AGN). They are characterized by the lack of strong emission lines, rapid variability at all wavelengths, and strong polarization. Their spectral energy distribution (SED), in the $\log \nu$ – $\log \nu F$ –representation, consists of a synchrotron component at lower frequencies and an inverse Compton component at higher frequencies. The peculiar traits of the BL Lac class are most likely caused by Doppler–boosted radiation emanating from a relativistic jet aligned close to the line of sight (Urry & Padovani 1995).

Traditionally, BL Lacs have been discovered in either radio or X-ray band, which led to their classification as radio-selected (RBL) and X-ray-selected (XBL) BL Lacs. Best-known RBL samples include the 1 Jy (Stickel et al. 1991), S4 (Stickel & Kühr 1994), and S5 (Kühr & Schmidt 1990) samples, and among the most important XBL samples are the EMSS (Gioia et al. 1990; Stocke et al. 1991) and Slew Survey (Perlman et al. 1996).

The two classes have different properties: RBLs are more variable, are more luminous at radio and optical wavelengths, and have a higher polarization (Stocke et al. 1985; Jannuzi et al. 1994). XBLs have a higher starlight fraction, 30−50% (Stocke et al. 1985), and their morphology is less core–dominated in the radio than that of RBLs (Perlman & Stocke 1993). Due to these differences, they were initially regarded as separate classes of AGN. However, in recent years samples including intermediate objects have been found in surveys which combine X-ray and radio observations. These include the RGB (RASS–Green Bank) sample (Laurent-Muehleisen et al. 1999), the Deep X-Ray Radio Blazar Survey (DXRBS) (Perlman et al. 1998; Landt et al. 2001), and the REX Survey (Caccianiga et al. 1999). Their discovery has strengthened the view that the BL Lac population is continuous and that RBLs and XBLs represent the opposite ends of the continuum. The reason for such a continuity lies in the cutoff frequency of the synchrotron component in the SED. The synchrotron peak frequency of RBLs is in the radio/IR band, and for XBLs the peak is mostly in

⋆ Table 3 and Fig. 13 are only available in electronic form at http://www.edpsciences.org

the UV/X-ray band (Giommi et al. 1995). The intermediate BL Lacs (IBL) have their synchrotron peak in the optical wavelengths. This explains why they were not observed in the first surveys. Following the synchrotron cutoff model, the terminology came to describe the physical difference of the two classes: the RBL / XBL -division was replaced by division into low-energy-peaked BL Lacs (LBL) and high-energy-peaked BL Lacs (HBL) (Padovani & Giommi 1995). Most RBLs are LBLs and most XBLs are HBLs, but not all. The class boundaries can be loosely defined as $\nu_{\rm peak} \approx 10^{13-14}$ Hz for LBLs, $\nu_{\rm peak} \approx 10^{15-16}$ Hz for IBLs, and $\nu_{\rm peak} \approx 10^{17-18}$ Hz for HBLs.

Fossati et al. (1998) linked the shape of the SED and the synchrotron peak frequency to the source luminosity: the lower the peak frequency, the more luminous the source. This would mean that LBLs are intrinsically more luminous than HBLs. This sequencing is based on the absence of high-luminosity HBLs and low-luminosity LBLs. However, recently Giommi et al. (2005) reported the possible discovery of high-luminosity HBLs in the Sedentary Survey, and evidence of low-power LBLs has also been discovered (Padovani et al. 2003; Caccianiga & Marchã 2004). These findings are at odds with the trend presented by Fossati et al.

Ghisellini (1999) suggested that there is a class of BL Lacs whose synchrotron peak lies at even higher frequencies than that of conventional HBLs, $\nu_{\rm peak} > 10^{19}$ Hz. These objects can be called ultra-high-energy synchrotron peak BL Lacs (UHBLs) (Giommi et al. 2001). Following the dependency of the SED shape and luminosity, UHBLs are thought to be extremely faint at radio wavelengths, which is why they have escaped notice. Extensive γ-ray observations are needed to unambiguously identify them.

In this paper we have taken a new approach to studying the properties of the BL Lac population. Our goal is to plot the SEDs of the Metsähovi Radio Observatory BL Lac sample, which comprises nearly 400 objects, including objects from all the best-known surveys at radio and X-ray wavelengths. This way we can examine the population properties of a sample with a wide range of attributes, instead of focusing on one or two limited surveys.

The aim of this paper was to test both the continuity of the BL Lac population and the blazar sequence scenario and to assign a SED-based classification to those objects that previously had none. A large database of flux measurements has been collected and SEDs are plotted for more than 300 BL Lacs. Each object is classified as LBL, IBL, or HBL. The relationship of synchrotron peak frequency and luminosities at several frequencies was also tested along with the properties of broad band spectral indices. Throughout this paper, we assume $H_0 = 65\,\mathrm{km\,s^{-1}\,Mpc^{-1}}$ and $\Omega_0 = 1$. All statistical tests were carried out using Unistat 5.5 software.

2. The sample

The Metsähovi BL Lac sample includes 381 objects selected from the Veron-Cetty & Veron BL Lac Catalogue (Veron-Cetty & Veron 2000), hereafter VCV2000, and 17 objects from the literature. Given the northern location of the Metsähovi observatory, the source with the lowest declination in the sample is PKS 2223-114 at $\delta = -11{:}13{:}41$. The list of sample sources (Table 3) is published electronically. A large part of the objects in VCV2000 are from well-known and well-defined samples such as the 1 Jy, S4, S5, EMSS, and the Einstein Slew Survey. The BL Lacs from the first release of DXRBS identifications (Perlman et al. 1998) are also included. No selection criteria (other than declination), in addition to the ones in the original surveys, were imposed on the sample. The aim was to examine the behaviour of an extensive sample containing all known BL Lacs up to the year 2000.

According to VCV2000, the Metsähovi BL Lac sample can be further classified as follows: 63% are confirmed, 3% probable and 8% possible BL Lacs, 14% are objects with high optical polarization, and 12% (including the BL Lacs taken from literature) lack any subclassification. In the sample there are 6 sources that are not in the later editions of the Veron-Cetty & Veron BL Lac Catalogues (Veron-Cetty & Veron 2001, 2003). These objects were excluded from the data analysis performed in this paper.

3. The data

In order to plot as accurate SEDs as possible, a large amount of data from several wavelengths was collected. Because simultaneous multifrequency flux measurements are not available, datapoints from different epochs were searched from databases and the literature.

3.1. Radio data

The starting point in collecting radio data were the Metsähovi observations at 37 GHz from late 2001 to January 2004. The full data set and a more detailed analysis of the 37 GHz behaviour of the sample sources will be published in a forthcoming paper (Nieppola et al., in preparation for A&A). Of the BL Lac sample, 137 objects were detected at $\sigma \geq 4$. There were 255 BL Lacs that were not detected and 6 that had not yet been observed during the time mentioned. The limiting flux of the Metsähovi radio telescope is about 0.2 Jy under optimal weather conditions.

Our group also obtained flux density data at higher radio frequencies from our observations with the Swedish-ESO Submillimetre Telescope (SEST) between 1987 and 2003 at 3 mm and 1.3 mm. For some objects we got data from the RATAN observatory at frequencies 2.3, 4.8, 7.7, 11.2, 21.8, and 30 GHz (Tornikoski et al., in preparation for A&A). Additional low frequency datapoints were found in VCV2000 and the WGA–catalogue (White et al. 1996).

The large majority of radio data were obtained from the Astrophysical Catalogues Support System (CATS) maintained by the Special Astrophysical Observatory, Russia[1]. The search results from CATS contained data from over 140 different catalogues and more than 100 radio frequencies.

[1] http://cats.sao.ru/

3.2. Data from other frequency bands

The IR datapoints are from CATS, originating from the IRAS- and 2MASS-catalogues. The wavelengths used are 1.25, 1.65, 2.0, 2.17, 12, 25, 60 and 100 μm. The optical data also are mainly from CATS. Some datapoints from V-band were added from Donato et al. (2001).

The X-ray data are from Einstein- and ROSAT-catalogues. The majority is from WGACAT (White et al. 1996) and the RBSC-catalogue (Voges et al. 1999). Datapoints were also collected from the following papers: Donato et al. (2001), Lamer et al. (1996), and Laurent-Muehleisen et al. (1999). EMSS-data were included as well (Gioia et al. 1990; Stocke et al. 1991). All of the data from gamma region came from the Third EGRET Catalogue (Hartman et al. 1999). Such data were available for only 14 objects.

4. Computing the SEDs

For all sources with a sufficient number of datapoints, a SED was plotted in the form $\log \nu - \log \nu F$. All frequencies used are observed frequencies and they have not been reduced to rest frame frequencies. The synchrotron component of the SED was fitted with a parabolic function

$$y = Ax^2 + Bx + C \quad (1)$$

in order to determine the synchrotron peak frequency $\nu_{\rm peak} = -B/2A$. The fitting was successful for 308 objects in total: the rest were too sparsely sampled. Among the fitted sources there were 4 which do not appear in the later versions of the Veron-Cetty & Veron catalogues of BL Lacertae objects, as mentioned in Sect. 2. Therefore they are not included in the analyses and discussion in this paper hereafter. The decision whether or not to include X-ray datapoints in the fit was based solely on a visual estimate for each individual object. All the SEDs (Fig. 13) are published electronically. The synchrotron peak frequencies are shown in Table 3 Col. 5.

We note that using a simple parabolic function in the fitting produces some error, especially among HBLs. In their case the X-ray datapoints are typically included in the rising synchrotron component, and therefore the parabola peaks after the X-ray domain. In reality, the synchrotron peak is expected to occur at or very close to the X-ray wavelengths and the decline to be more rapid. Thus the peak frequencies of the most extreme objects can be exaggerated.

The objects were assigned an LBL/IBL/HBL classification according to $\nu_{\rm peak}$. On the basis of the criteria of Padovani & Giommi (1995), we decided to draw the boundaries as follows: for LBLs, $\log \nu_{\rm peak} < 14.5$, for IBLs $14.5 < \log \nu_{\rm peak} < 16.5$, and for HBLs $\log \nu_{\rm peak} > 16.5$. Thus the peak frequencies of LBLs stretch up to the optical region, IBLs peak in the optical and UV-bands and HBLs from soft X-rays upwards.

4.1. The distribution of $\nu_{\rm peak}$

When the objects were classified as LBL/IBL/HBL according to their $\nu_{\rm peak}$, as described in the previous section, the division resulted in the three classes being almost equal in size. There were 98 LBLs, 96 IBLs, and 110 HBLs. The distribution is smooth and decreases steadily towards the higher peak frequencies (Fig. 1). This can be a real effect, suggesting that sources in which electrons are accelerated to extreme energies are intrinsically rare or are due to selection effects in surveys. The frequency interval $\nu_{\rm peak} = 10^{13-14}$ Hz is the most populated.

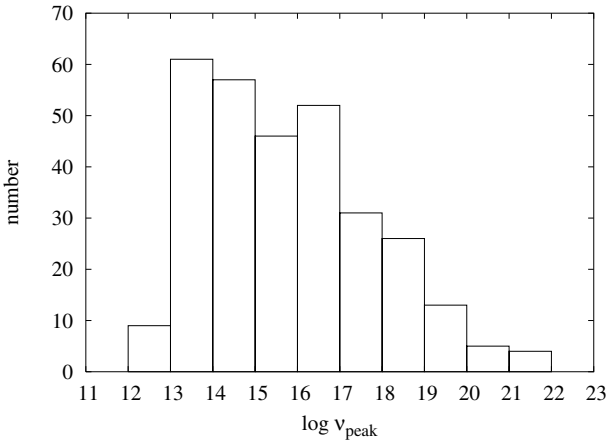

Fig. 1. The distribution of the synchrotron peak frequencies in the Metsähovi sample.

Table 1. Division of observational BL Lac classes to physical ones.

	LBL	IBL	HBL
RBL	84%	10%	6%
IBL	22%	36%	42%
XBL	21%	25%	54%

Table 1 presents how the classification with respect to the observational band relates to the one based on the SED. Here RBL classification has been assigned to objects in the 1 Jy and S4 surveys, IBL to objects in RGB and 200 mJy BL Lac (Bondi et al. 2001) surveys, and XBL to objects in the Einstein Slew Survey. This RBL/XBL classification has been adopted from Giommi et al. (1995). Among the 304 sources for which the SED could be plotted, there were 31 RBLs, 115 IBLs, and 48 XBLs. Several objects got multiple classifications.

Table 1 clearly demonstrates how surveys in the X-ray energies are more prone to finding low-energy BL Lacs than radio surveys are to finding HBLs. A large majority of RBLs really are LBLs. In fact, the 6% of RBLs that turned out to be HBLs are the radio-luminous Mrk 421 and Mrk 501. Objects in the RGB and 200 mJy samples are more likely to be HBLs than LBLs, and only a third of them are truly intermediate. Of the XBLs, only half are HBLs and over 20% are actually low-energy BL Lacs. These figures are certainly affected by the arbitrariness of the dividing boundaries between the classes, but the overall trend is expected to remain. It results from the fact that the X-ray luminosities of the samples in question are roughly the same, whereas radio luminosities differ greatly.

Table 2. Objects for which $\log \nu_{\rm peak} > 19$.

Source	RA (J2000)	Dec (J2000)	$\log \nu_{\rm peak}$
1ES 0229+200	02:32:48.6	+20:17:17	19.45
RXS J0314.3+0620	03:14:23.9	+06:19:57	19.57
2E 0323+0214	03:26:13.9	+02:25:14	19.87
2E 0414+0057	04:16:52.4	+01:05:24	20.71
1ES 0502+675	05:07:56.1	+67:37:24	19.18
EXO 0706.1+5913	07:10:30.1	+59:08:21	21.05
RXS J0847.2+1133	08:47:12.9	+11:33:52	19.13
1ES 0927+500	09:30:37.5	+49:50:25	21.13
RXS J1008.1+4705	10:08:11.3	+47:05:20	19.67
RXS J1012.7+4229	10:12:44.3	+42:29:57	20.97
EXO 1449.9+2455	11:49:30.3	+24:39:27	19.83
PG 1218+304	12:21:21.9	+30:10:37	19.14
RXS J1319.5+1405	13:19:31.7	+14:05:34	20.85
RXS J1341.0+3959	13:41:05	+39:59:45	20.06
RXS J1353.4+5601	13:53:28	+56:00:55	19.23
RXS J1410.5+6100	14:10:31.7	+61:00:10	20.25
2E 1415+2557	14:17:56.6	+25:43:25	19.24
RXS J1456.0+5048	14:56:03.7	+50:48:25	19.94
RXS J1458.4+4832	14:58:28	+48:32:40	21.46
1ES 1533+535	15:35:00.8	+53:20:37	19.68
RXS J1756.2+5522	17:56:15.9	+55:22:18	19.90
RXS J2304.6+3705	23:04:36.6	+37:05:08	21.01

4.2. UHBL candidates

As Fig. 1 shows, there were several objects in the sample whose synchrotron peak frequency was extremely high. Usually objects with $\log \nu_{\rm peak} > 17$ are considered as extreme; here the number of such objects was 80, approximately 26% of all the fits. For 22 objects $\log \nu_{\rm peak} > 19$ (Table 2) and for 9 objects even $\log \nu_{\rm peak} > 20$, corresponding to a peak energy of ~0.4 MeV. The SEDs of these sources were, on the whole, very sparsely sampled, typically with datapoints from radio, optical, and X-ray bands, and should be treated with caution. That said, we note that even for objects with $\log \nu_{\rm peak} > 20$, the datapoints fit very well on the rising parabolic function. We note again that the actual position of the peak is probably exaggerated by the use of a parabolic fitting function, as mentioned in Sect. 4, meaning the peak frequencies of these objects cannot be considered as definite. Because they peak near the MeV-region, these sources would be excellent candidates for γ-observations.

5. Correlation between $\nu_{\rm peak}$ and luminosity

5.1. High radio frequency (37 GHz)

Out of the three BL Lac classes, LBLs had 37 GHz detections for 81% of the sources, IBLs for 36%, and HBLs for 12%. This seems to indicate that most HBLs have a radio flux well below the flux limit of the Metsähovi telescope. This prompted us to study the possible correlation between synchrotron peak frequency and 37 GHz source luminosity more closely.

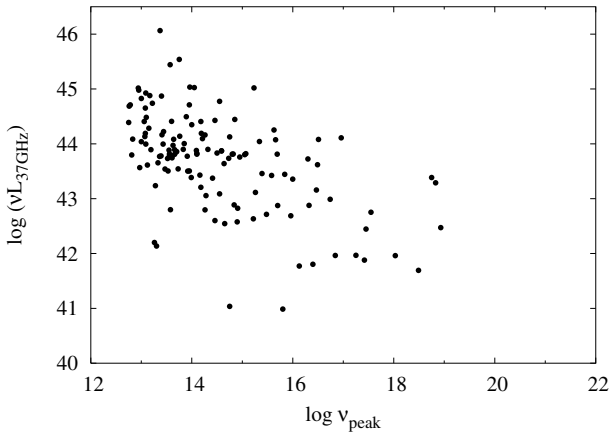

Fig. 2. Radio luminosity at 37 GHz plotted against synchrotron peak frequency.

To calculate the luminosities, redshift data was collected from VCV2000, Stocke et al. (1991), Laurent-Muehleisen et al. (1999), Donato et al. (2001), and the SIMBAD database[2]. For sources with no redshift available, we used $z = 0.4$. Both a detection at 37 GHz and synchrotron peak frequency $\nu_{\rm peak}$ were available for 132 objects.

[2] `http://simbad.u-strasbg.fr`

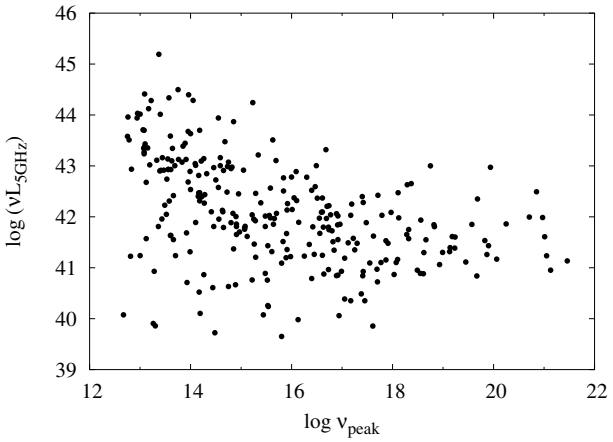

Fig. 3. Radio luminosity at 5 GHz plotted against synchrotron peak frequency.

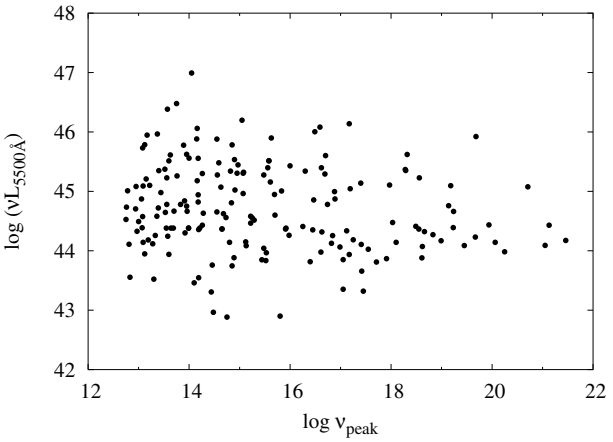

Fig. 4. Optical luminosity at 5500 Å plotted against synchrotron peak frequency.

When the 37 GHz luminosity is plotted against the synchrotron peak frequency (Fig. 2), the correlation is easily seen. LBLs are at the high-luminosity end of the plot, and the luminosity drops towards the high-energy regime. According to the Spearman Rank Correlation Test, there is significant negative correlation at the 99% confidence level.

No real evidence of a population of low-luminosity LBLs or high-luminosity HBLs was found. However, there are two LBLs with luminosities that are almost as low as those of HBLs, disrupting the declining trend. In addition, the lowest luminosities are not claimed by objects at the high end of the peak frequency range, but by two IBLs with $\log \nu_{\rm peak} < 16$. The radio luminosities are widely scattered. An object with $\log \nu L = 44$ can have peak frequency values ranging from $\log \nu_{\rm peak} = 13$ to $\log \nu_{\rm peak} = 17$, approximately. Thus the radio luminosity cannot be used to determine the peak frequency of the source.

5.2. Low radio frequency (5 GHz)

The small number of HBL datapoints at 37 GHz convinced us to also test the correlation at 5 GHz. The number of available datapoints rose to 280, and the correlation plot changed drastically (Fig. 3). The most noticeable difference is the appearance of several low-luminosity LBLs (lower left of the figure). They even reach lower luminosities than any of the HBLs. The overall negative correlation is still present and significant at a 99% level. This differs from the result obtained by Padovani et al. (2003). However, their DXRBS BL Lac sample consisted of only 31 objects that mainly represent the LBL/IBL end of the plot. This is the region with the most scatter in our figure, and within this limited area, the correlation is less obvious even with a larger number of datapoints. Only when the whole range of values of $\log \nu_{\rm peak}$ is considered does the trend become evident.

When compared with the corresponding figure of Fossati et al. (1998), our figure has much more scatter. A part of it is caused by a larger number of datapoints, but on closer examination, our $\log \nu_{\rm peak}$ values for the Slew Survey are spread much more widely. In Fossati et al. (1998), the Slew Survey objects have $\log \nu_{\rm peak} = 15{-}19$, while in our study they have $\log \nu_{\rm peak} \approx 13{-}21$. The 1 Jy–sample takes on similar peak frequency values in both studies.

We note that there is no evidence of very high-luminosity HBLs. In fact, the extreme HBLs adopt quite intermediate luminosity values also avoiding the low-luminosity region. However, the spectra of possible high-luminosity HBLs would very likely be totally featureless because of the powerful nucleus, and thus the object would lack a redshift estimation. Therefore the redshift value assigned to featureless sources could have a big impact on the luminosity correlations and the appearance of high-luminosity HBLs (see Sect. 5.6).

5.3. Optical region (5500 Å)

Figure 4 shows the optical luminosity at wavelength 5500 Å plotted against $\log \nu_{\rm peak}$. There is a significant, slightly negative correlation present at a 95% level. We see again that LBLs have more scatter than HBLs. Overall, the correlation is much less evident than in the case of radio luminosity.

5.4. X-ray region

In Fig. 5 we have plotted the correlation between X-ray luminosity and $\log \nu_{\rm peak}$. In calculating the luminosities we used both 1 keV data and data from the ROSAT band (0.1−2.4 keV). The error produced by the bandwidth difference is negligible when only the statistical properties of a large sample are considered. We note that in the case of X-ray luminosity, the correlation is positive and significant at a 99% level. This contrasts with the blazar sequence scenario. Fossati et al. (1998) state that the overall luminosity of HBLs is lower than that of LBLs (see their Fig. 12). While they admit that in the X-ray band objects exhibit complex behaviour, the systematic rising trend presented by our findings is not predicted.

5.5. Peak luminosity $L_{\rm peak}$

In addition to luminosities at defined frequency bands, we calculated the luminosity at the synchrotron peak frequency for

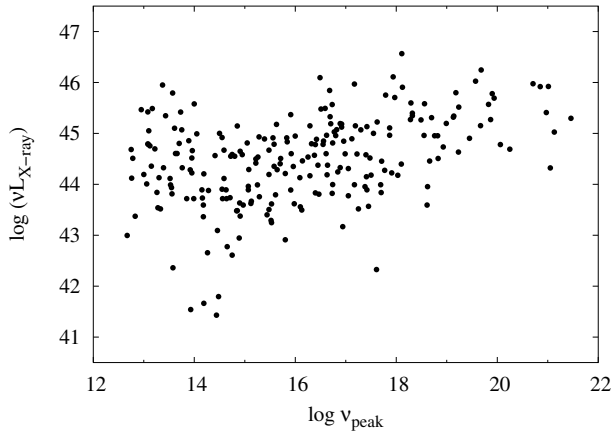

Fig. 5. X-ray luminosity at 1 keV and ROSAT band plotted against synchrotron peak frequency.

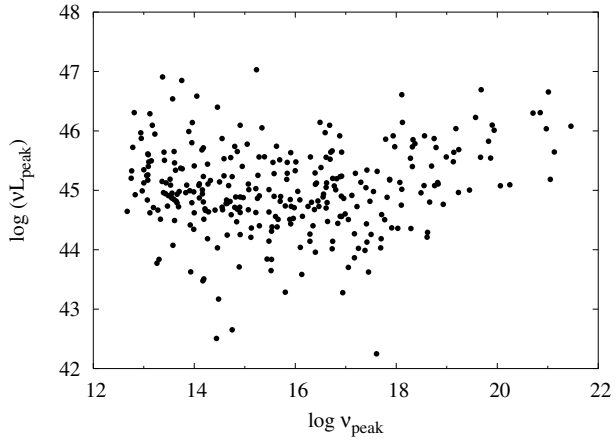

Fig. 6. Luminosity at the synchrotron peak frequency plotted against synchrotron peak frequency.

each source. This is plotted against $\log \nu_{\rm peak}$ in Fig. 6. There is no significant correlation, so that we can decisively say that the source luminosity does not depend on the synchrotron peak frequency. Figure 7 of Fossati et al. (1998) also shows the dependence of $L_{\rm peak}$ and $\log \nu_{\rm peak}$. In their study there is a significant, yet weak correlation. Again, we notice that a larger number of datapoints and a wider range of $\log \nu_{\rm peak}$ reveal the true behaviour of the population and the lack of correlation. If only objects with $\log \nu_{\rm peak} < 17$ are considered, there is a weak negative correlation in our sample also. On the other hand, when the high-energy tail with $\log \nu_{\rm peak} > 17$ is tested, we find a significant positive correlation. Therefore the distribution almost seems to assume a concave shape.

5.6. The effect of z on luminosity correlations

Giommi et al. (2005) found numerous candidates for high-luminosity HBLs in the Sedentary Survey. All these objects seemed to reside at high redshifts ($z \geq 0.7$). In our luminosity calculations we assumed $z = 0.4$ for featureless objects, which is a low value compared to Giommi et al. Using too low a redshift value for a significant part of the sources would lead to a serious underestimation of luminosities. To take this into account, we also tested the luminosity correlations by assigning redshifts $z = 0.7$, $z = 1$, and $z = 1.5$ to those objects that had none.

The effect was most pronounced in the case of radio luminosities at 5 and 37 GHz. The number of relatively high-luminosity HBLs increased with the higher assumed redshift. However, only at very high reshift values ($z = 1$ or $z = 1.5$) did the luminosities of a few HBLs become roughly comparable to those of LBLs. Considering the population average, $z_{\rm av} = 0.33$, it is questionable whether all featureless sources would have $z \geq 1$, although for some of them this may be the case. Therefore, while the existence of high-luminosity HBLs in this sample is possible, we do not expect the correlations to be affected by them.

In other frequency bands than radio, the effect of an increasing redshift was negligible. The shape of the correlations did not change notably, while the scatter increased somewhat. We note that in all wavelengths and for all assumed redshift values, the significance of the statistical correlations remained the same.

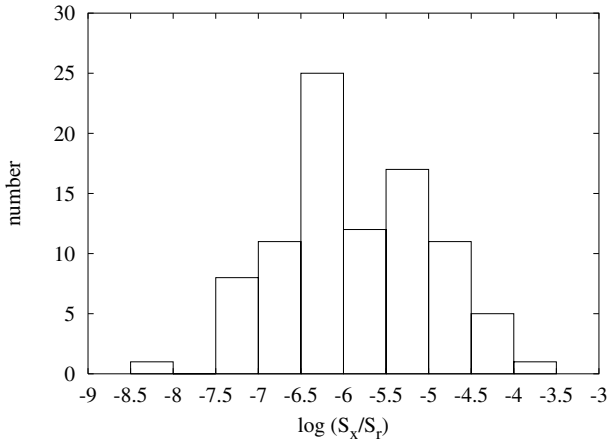

Fig. 7. The distribution of $\log (S_x/S_r)$.

6. Other properties of the sample

6.1. Log(S_x/S_r)-distribution

The $\log (S_x/S_r)$-distribution has traditionally been used to point out the bimodality in the BL Lac population. The dividing line between RBLs and XBLs has been $\log (S_x/S_r) = -5.5$ (Laurent-Muehleisen et al. 1999), when the fluxes are in the same units and X-ray and radio frequencies are 0.1−2.4 keV and 5 GHz, respectively. Here we calculated the distribution to check the assumed continuity of the sample. X-ray fluxes are from the ROSAT band 0.1−2.4 keV, and radio measurements are from Metsähovi at 37 GHz. If there was more than one flux measurement from one frequency, the average value was used.

The distribution is indeed unbroken with an average of $\log (S_x/S_r) = -5.85$ (Fig. 7). The most populated interval is $\log (S_x/S_r) = [-6, -6.5]$. Pertaining to the unbalanced detection rates at 37 GHz, LBLs are overrepresented compared to HBLs in the plot. Only 14% of the objects are HBLs. When considered separately, LBLs, IBLs, and HBLs move

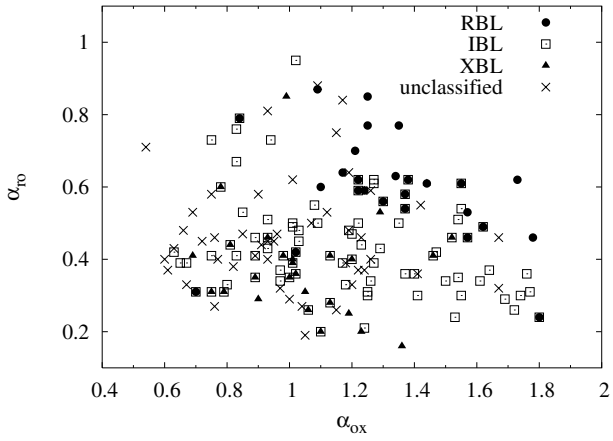

Fig. 8. The colour plane: α_{ro} plotted against α_{ox}. Frequency intervals 5 GHz–5500 Å–1 keV, ROSAT band. Different symbols denote the observational classification of BL Lacs.

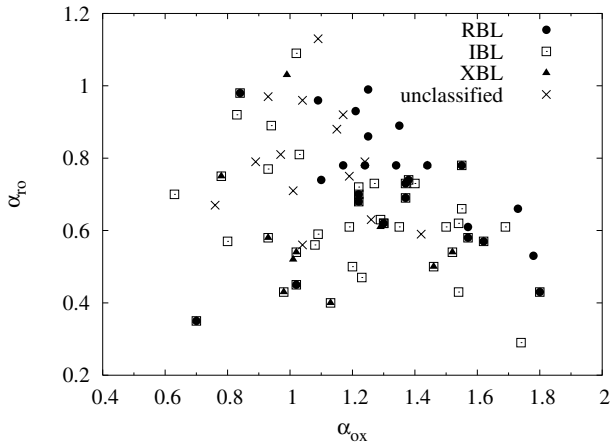

Fig. 9. The colour plane: α_{ro} plotted against α_{ox}. Frequency intervals 37 GHz–5500 Å–1 keV, ROSAT band. Different symbols denote the observational classification of BL Lacs.

progressively from low to higher values of $\log(S_x/S_r)$. There is substantial overlap between the distributions. The average values are −6.35, −5.50, and −4.85 for LBLs, IBLs, and HBLs respectively.

6.2. Broad band spectral indices

6.2.1. The $\alpha_{ro} - \alpha_{ox}$ diagram

We calculated broad band spectral indices α_{ro} and α_{ox} to plot the sample in α_{ro} vs. α_{ox} diagram. Here the spectral index is defined as

$$\alpha_{1-2} = -\frac{\log(S_1/S_2)}{\log(\nu_1/\nu_2)} \quad (2)$$

where S_1 and S_2 are the fluxes in frequencies ν_1 and ν_2, respectively, and $S_\nu = \nu^{-\alpha}$.

The α_{ro} vs. α_{ox} diagram has also been used as a means to demonstrate the division of the population. Generally, XBLs have lower values for both indices occupying the lower left corner of the plot, whereas RBLs lie in the upper right corner (Stocke et al. 1985; Laurent-Muehleisen et al. 1999). IBLs seem to have bridged the gap with intermediate values of both indices.

For comparison, we plotted two diagrams; one with low radio frequency (5 GHz) (Fig. 8) and one with high radio frequency (37 GHz) (Fig. 9). The optical wavelength used was 5500 Å. In both diagrams we used X-ray data at 1 keV from the literature and, in addition, data from ROSAT band 0.1−2.4 keV. The error produced by the bandwidth difference is small compared with the benefits of a larger number of datapoints.

When the lower radio frequency is used (Fig. 8), the indices for the whole population are $\alpha_{ox} = 0.54-1.8$ and $\alpha_{ro} = 0.16-0.95$. RBLs and XBLs occupy their expected locations, but overall the distribution is even.

As for the higher radio frequency diagram (Fig. 9), the intervals are slightly different: $\alpha_{ox} = 0.63-1.8$ and $\alpha_{ro} = 0.29-1.13$. The values of α_{ox} are the same as in Fig. 8, but the number of datapoints is smaller. Here we note again the lack of HBLs compared to LBLs. This is why the lower left corner of Fig. 9 is underpopulated compared with Fig. 8.

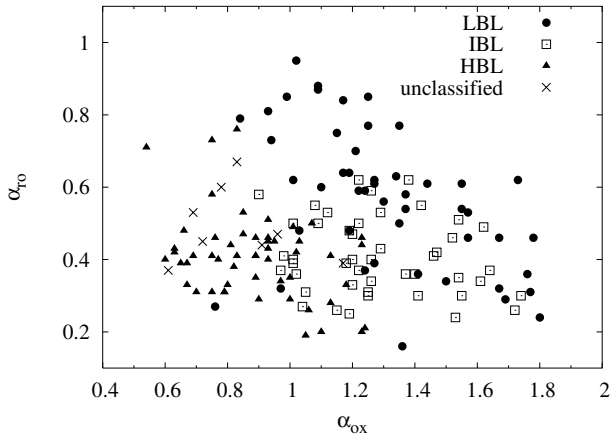

Fig. 10. The colour plane: α_{ro} plotted against α_{ox}. Frequency intervals 5 GHz−5500 Å–1 keV, ROSAT band. Different symbols denote the physical classification of BL Lacs obtained in this study.

We also plotted the diagram with 5 GHz showing the LBL/IBL/HBL classification of our study (Fig. 10). It clearly shows how the transition of the synchrotron peak from LBL to HBL moves the object on the $\alpha_{ro} - \alpha_{ox}$–plane from the top to lower right and onwards to lower left, as described by Padovani & Giommi (1995). However, there are several LBLs that appear on the wrong side of the $\alpha_{rx} = 0.75$ line that has usually been thought of as a dividing line between LBLs and HBLs. This suggests that the $\alpha_{rx} = 0.75$ divide is not very effective and LBLs take on very scattered values of α_{ro}.

There are some objects in the $\alpha_{ro} - \alpha_{ox}$–plot (Fig. 10) with no classification (marked with x). They are concentrated in quite a small area with $\alpha_{ox} = 0.61-1.17$ and $\alpha_{ro} = 0.37-0.67$. Their synchrotron peak frequencies have not been calculated on account of very poor fits, but judging by their spectral indices they are likely to be HBLs.

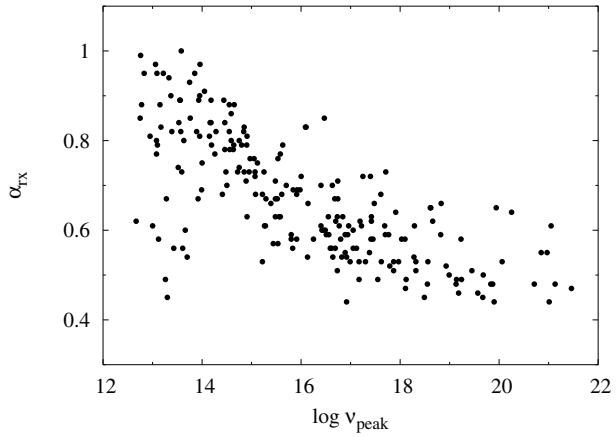

Fig. 11. Radio-X-ray spectral index α_{rx} plotted against synchrotron peak frequency.

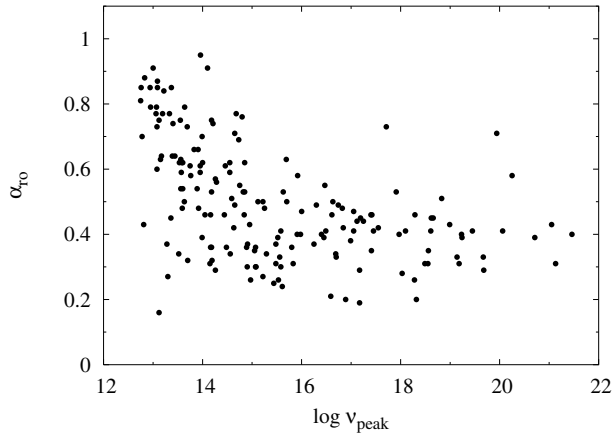

Fig. 12. Radio-optical spectral index α_{ro} plotted against synchrotron peak frequency.

6.2.2. α_{rx} vs. log ν_{peak}

The relation between α_{rx} and $\log \nu_{peak}$ is shown in Fig. 11. We used radio frequency 5 GHz, and X-ray data comes primarily from 1 keV. For those objects that have no 1 keV flux available, we used data from the ROSAT band. According to the Spearman rank correlation test, the negative correlation is significant at a 99% level. However, the correlation seems to break apart at $\log \nu_{peak} < 14$. LBLs take on α_{rx}–values between 0.45−1. Fossati et al. (1998) suggested that the correlation between the radio luminosity and X-ray luminosity in the rising Compton–component makes α_{rx} tend to a fixed value when $\log \nu_{peak} < 14$, but in our plot this seems not to be the case.

When $\log \nu_{peak} > 14$, the correlation is apparent. This speaks for the authenticity of the UHBL candidates, as they take their place at the end of the continuum with low spectral index values. All objects with $\log \nu_{peak} > 19$ also have $\alpha_{rx} \leq 0.65$.

From the α_{rx} vs. $\log \nu_{peak}$–plot, we can see that assigning an object an LBL/HBL classification based only on the value of α_{rx} is risky. While an object with $\alpha_{rx} > 0.75$ is very likely an LBL, the opposite does not hold. In fact, approximately 30% of objects with $\alpha_{rx} < 0.75$ have $\log \nu_{peak} < 16$. At $\alpha_{rx} \approx 0.6$ the possible values of ν_{peak} span as much as eight magnitudes.

When compared with the corresponding figures of Fossati et al. (1998) and Padovani et al. (2003), our plot seems to be a combination of the two. This is explained by the fact that both the samples used by Fossati et al. (1 Jy and Slew Survey) and part of the sample used by Padovani et al. (DXRBS) are included in the Metsähovi sample. Thus we see a strong correlation with a substantial increase in scatter of the α_{rx}–values towards the lower end. We stress that our data considerably extends the range of values of $\log \nu_{peak}$.

6.2.3. α_{ro} vs. log ν_{peak}

The correlation between (i) the spectral index between radio (5 GHz) and optical (5500 Å) frequencies and (ii) synchrotron peak frequency is shown in Fig. 12. The overall trend is easily seen as it changes from the steep negative correlation of LBLs to an almost constant trend of HBLs. The change occurs roughly when the synchrotron peak of the SED moves to frequencies higher than those used to calculate α_{ro}. After that point, the peak frequency no longer has an influence on α_{ro}. The negative correlation is significant at a 99% level. Again, however, we see a few points breaking this scenario, both LBLs with very low values of α_{ro} and HBLs with high values of α_{ro}.

We note that, as in the case of α_{rx}, the scatter in the figure is significant. Therefore the value of α_{ro} cannot be reliably used to classify BL Lacs. Only if α_{ro} is very close to one, the object is likely to be an LBL.

7. Discussion

Our findings support the results of Costamante et al. (2001). Their study concludes that objects 1ES 0033+595, 1ES 0120+340, 1ES 1218+304, and 1ES 1426+428 are extreme HBLs with synchrotron peak frequencies exceeding 10^{18} Hz. Our results show that they all peak at roughly $\log \nu_{peak} \approx 19$. Meanwhile, the extreme nature of 1ES 2344+514 (Giommi et al. 2000) is not revealed in our study, as it had a peak frequency of $\log \nu_{peak} = 16.4$. Giommi et al. state that it is indeed very variable, with synchrotron peak frequencies ranging from $\log \nu_{peak} \approx 17$ to $\log \nu_{peak} \approx 18$. Mrk 501 is another example of a variable source; its synchrotron peak has been as high as $\log \nu_{peak} \approx 19$ (Pian et al. 1998), but the peak in our SED occured at $\log \nu_{peak} \approx 16.84$.

In this paper we tested the correlation between the synchrotron peak frequency and luminosities at radio, optical, and X-ray wavelengths, along with luminosity at the synchrotron peak of each source. According to the blazar sequence scenario promoted by Fossati et al. (1998), HBLs have lower luminosities at all wavelenghts. In the X-ray region, in the SED of LBLs the synchrotron and SSC–components meet, resulting in a concave X-ray spectrum. In HBLs the synchrotron component peaks at or near the X-ray energies. Because the SEDs of LBLs and HBLs are so differently shaped in this frequency band, the X-ray correlation may be less significant. Still, on the whole, LBLs are expected to be more luminous. When the defined

frequency bands are considered, our data seems to support this scenario in all other frequencies except in X-rays. There we find a clear positive correlation that contradicts the blazar sequence. Luminosities rise towards the high peak frequencies. When all luminosity vs. $\log \nu_{\rm peak}$ correlations are studied simultaneously, a kind of sequence is revealed: at radio frequencies the negative correlation is steep, in optical wavelengths the correlation is only slightly negative, and in the X-ray region it turns positive. However, the negative correlation of luminosity at 5 GHz and synchrotron peak frequency is expected to originate solely from the shifting of the bulk of the synchrotron emission to the higher frequencies with growing $\log \nu_{\rm peak}$ and, as such, does not authenticate the interdependence of source luminosity and peak frequency. A negative luminosity correlation at 5 GHz and a positive one at X-ray energies is what we would expect, if the only parameter to change in the SED sequence was $\nu_{\rm peak}$. When source luminosities at synchrotron peak frequencies are calculated, we find that they do not correlate with $\log \nu_{\rm peak}$.

In addition to the positive correlation of X-ray luminosity and synchrotron peak and the lack of synchrotron luminosity correlation, the blazar sequence scenario is brought into question by the appearance of numerous low-luminosity LBLs at 5 GHz. The faintest LBLs reach even lower luminosities than most of the HBLs. As the 5 GHz flux limit of even the least limited radio-selected sample, RGB, is 20 mJy, it is obvious that these objects have been identified for the most part from X-ray surveys. We note that there are some 5 GHz low-luminosity LBLs that have a detection at 37 GHz. Especially for these sources, we have to consider the possibility that the 5 GHz flux measurement is from a particularly quiescent state and does not represent the object accurately. Padovani et al. (2003) found low-luminosity LBLs among the DXRBS BL Lacs. In our low-luminosity LBLs there are 4 objects from the DXRBS survey.

The 5 GHz low-luminosity LBLs also appear in luminosity plots from other frequency bands, again at the low-luminosity end. All the extreme HBLs have relatively high or intermediate luminosities. This effect, especially in X-rays, seems to support the scenario that UHBLs are in fact a rare class. If they were common and X-ray luminous, the numerous X-ray surveys performed lately should have detected them in large numbers. On the whole, the scatter in luminosities diminishes towards higher peak frequencies at all wavelengths. There is no solid evidence of truly high-luminosity HBLs with a measured redshift in radio wavelengths. The high-luminosity HBLs reported by Giommi et al. (2005) are from the Sedentary Survey, which is not included in our sample.

We find that the low-luminosity LBLs also behave abnormally on the broad band spectral index plots, $\alpha_{\rm ro}$ vs. $\alpha_{\rm ox}$, $\alpha_{\rm rx}$ vs. $\log \nu_{\rm peak}$, and $\alpha_{\rm ro}$ vs. $\log \nu_{\rm peak}$. In the first the BL Lac classes take their expected places except for a few of the low-luminosity LBLs that invade the region usually populated by HBLs. Doing so, they cross the $\alpha_{\rm rx} = 0.75$ border frequently used to classify BL Lacs to LBLs and HBLs.

When the $\alpha_{\rm rx}$ vs. $\log \nu_{\rm peak}$–plot is examined, we find a strong negative correlation, but LBLs ($\log \nu_{\rm peak} < 14$) disrupt the trend and take on values $\alpha_{\rm rx} = 0.45-1$. Hints of such a distribution was discovered by Padovani et al. (2003), but the wider range of $\log \nu_{\rm peak}$ in our sample makes it evident. All LBLs with conspicuously low $\alpha_{\rm rx}$ are among the low-luminosity LBLs in the 5 GHz luminosity plot. We considered the possibility that the low indices in these objects are due to the wider bandwidth of the ROSAT fluxes compared to the 1 keV fluxes, but this seems to have little effect. For those objects that had $\alpha_{\rm rx}$ computed for both X-ray energies, we calculated the average values of both indices. The average for ROSAT band $\alpha_{\rm rx}$ was 0.63, while for 1 keV fluxes it was 0.69. This difference is small compared to the deviation of the low-$\alpha_{\rm rx}$ LBLs from their expected location. Also for 3 of the 10 LBLs with lowest $\alpha_{\rm rx}$-values, 1 keV flux has been used in calculating the spectral index.

In the $\alpha_{\rm ro}$ vs. $\log \nu_{\rm peak}$–plot, LBLs behave in a similar way; at $\log \nu_{\rm peak} \approx 13$ they have $\alpha_{\rm ro} = 0.16-0.95$. In this plot we also see 3 HBLs with conspicuously high $\alpha_{\rm ro}$. They have relatively high radio luminosities and low optical luminosities. Each source has only one flux measurement at 5500 Å, possibly from an anomalously quiescent state. For these HBLs we also considered the possibility that their X-ray flux actually originates from IC rather than synchrotron radiation. This would lower their peak frequencies and move them left on the $\alpha_{\rm ro}$ vs. $\log \nu_{\rm peak}$-plane. For two of them (RXS J1456.0+5048, $\log \nu_{\rm peak} = 19.94$ and RXS J1410.5+6100, $\log \nu_{\rm peak} = 20.25$), this seems possible albeit uncertain.

As explained before, when there are few datapoints representing the SED, the peak frequency is easily overestimated in the case of extreme HBLs. This also affects the luminosity correlations. However we do not expect the significance of the correlations at defined wavelengths to change, even if the datapoints in the high-energy end moved to the left. The only case where the consequences could be substantial is the $\log L_{\rm peak}$ vs. $\log \nu_{\rm peak}$-plot (Fig. 6). If the peak frequency is exaggerated, so is the luminosity at peak frequency. Thus the uncertain datapoints can move from upper right to lower left, possibly changing the correlation. We tested this by artificially lowering the peak luminosities of those sources whose $\nu F_{\rm peak}$ was notably higher in the SED than their X-ray flux, $\nu F_{\rm X-ray}$. We changed their peak frequencies accordingly, and the highest $\log \nu_{\rm peak}$ in the sample changed from 21.46 to 19.44, yet the overall shape of the plot did not change enough to produce significant correlation. Therefore we find it unlikely that this overestimation of the $\log \nu_{\rm peak}$ of HBLs affects the main results of this study.

8. Conclusions

In this paper we collected a large amount of multifrequency data, as well as new flux measurements at 37 GHz, and plotted the spectral energy distributions of over 300 BL Lacs of the Metsähovi BL Lac sample. Using such an extensive sample allowed us to detect the whole range of synchrotron peak frequencies reaching up to the MeV-region. The main conclusions are as follows:

1. For 22 objects we find that $\log \nu_{\rm peak} > 19$. This high-frequency tail of the $\nu_{\rm peak}$ distribution is unrepresented in

most previous studies, but we find it essential for determining the properties of the population accurately.
2. The positive correlation of X-ray luminosity and synchrotron peak frequency and the lack of correlation between the source luminosity at synchrotron peak and peak frequency contradict the blazar sequence scenario. The differences between LBLs and HBLs cannot be attributed to unequal luminosities.
3. When the broad band spectral indices $\alpha_{\rm rx}$ and $\alpha_{\rm ro}$ are plotted against $\log \nu_{\rm peak}$, we find substantial scatter in the figures. This implies that the values of $\alpha_{\rm rx}$ and $\alpha_{\rm ro}$ cannot be reliably used in BL Lac classification.
4. Based on the smooth, declining distribution of $\nu_{\rm peak}$ and the lack of any bimodality in all other tests and calculations, we conclude that the BL Lac population as a whole is continuous and undivided.

Acknowledgements. We gratefully acknowledge the funding from the Academy of Finland for our Metsähovi and SEST observing projects (project numbers 205969, 46341, and 51436). E.N. thanks Ilona Torniainen for help in producing the SED plots for publication.

References

Bondi, M., Marchã, M. J. M., Dallacasa, D., & Stanghellini, C. 2001, MNRAS, 325, 1109
Caccianiga, A., Maccacaro, T., Wolter, A., della Ceca, R., & Gioia, I. M. 1999, ApJ, 513, 51
Caccianiga, A., & Marchã, M. J. M. 2004, MNRAS, 348, 937
Costamante, L., Ghisellini, G., Giommi, P., et al. 2001, A&A, 371, 512
Donato, D., Ghisellini, G., Tagliaferri, G., & Fossati, G. 2001, A&A, 375, 739
Fossati, G., Maraschi, L., Celotti, A., Comastri, A., & Ghisellini, G. 1998, MNRAS, 299, 433
Ghisellini, G. 1999, ApL&C, 39, 17
Gioia, I., Maccacaro, T., Schild, R., et al. 1990, ApJS, 72, 567
Giommi, P., Ansari, S. G., & Micol, A. 1995, A&AS, 109, 267
Giommi, P., Padovani, P., & Perlman, E. 2000, MNRAS, 317, 743
Giommi, P., Ghisellini, G., Padovani, P., & Tagliaferri, G. 2001, AIPC, 599, 441
Giommi, P., Piranomonte, S., Perri, M., & Padovani, P. 2005, A&A, 434, 385
Hartman, R. C., Bertsch, D. L., Bloom, S. D., et al. 1999, ApJS, 123, 79
Jannuzi, B. T., Smith, P. S., & Elston, R. 1994, ApJ, 428, 130
Kühr, H., & Schmidt, G. 1990, AJ, 99, 1
Lamer, G., Brunner, H., & Staubert, R. 1996, A&A, 311, 384
Landt, H., Padovani, P., Perlman, E. S., et al. 2001, MNRAS, 323, 757
Laurent-Muehleisen, S. A., Kollgaard, R. I., Feigelson, E. D., Brinkmann, W., & Siebert, J. 1999, ApJ, 525, 127
Padovani, P., & Giommi, P. 1995, ApJ, 444, 567
Padovani, P., Perlman, E. S., Landt, H., Giommi, P., & Perri, M. 2003, ApJ, 588, 128
Perlman, E. S., Padovani, P., Giommi, P., et al. 1998, AJ, 115, 1253
Perlman, E. S., & Stocke, J. T. 1993, ApJ, 406, 430
Perlman, E. S., Stocke, J. T., Schachter, J. F., et al. 1996, ApJS, 104, 251
Pian, E., Vacanti, G., Tagliaferri, G., et al. 1998, ApJ, 492, 17
Stickel, M., & Kühr, H. 1994, A&AS, 103, 349
Stickel, M., Padovani, P., Urry, C. M., Fried, J. W., & Kühr, H. 1991, ApJ, 374, 431
Stocke, J. T., Liebert, J., Schmidt, G., et al. 1985, ApJ, 298, 619
Stocke, J. T., Morris, S. L., Gioia, I. M., et al. 1991, ApJS, 76, 813
Urry, C. M., & Padovani, P. 1995, PASP, 107, 715
Veron-Cetty, M. P., & Veron, P. 2000, ESOSR, 19, 1
Veron-Cetty, M. P., & Veron, P. 2001, A&A, 374, 92
Veron-Cetty, M. P., & Veron, P. 2003, A&A, 412, 399
Voges, W., Aschenbach, B., Boller, T., et al. 1999, A&A, 349, 389
White, N. E., Giommi, P., & Angelini, L. 1996, VizieR Online Data Catalogue IX/12, 9012, 0

Online Material

Table 3. The Metsähovi BL Lac sample. The synchrotron peak frequency and subsequent classification designated in this study are included when available.

Source	RA(J2000)	Dec(J2000)	$\log \nu_{\rm peak}$	Class
NRAO 5	00:06:13.9	–06:23:36	12.75	LBL
RX J0007.9+4711	00:07:59.9	47:12:07	16.14	IBL
MS 0011.7+0837	00:14:19.7	08:54:04	16.74	HBL
RXS J0018.4+2947	00:18:27.8	29:47:32	–	–
PKS 0017+200	00:19:37.9	20:21:46	13.08	LBL
PKS 0019+058	00:22:32.5	06:08:05	13.19	LBL
RXS J0325.2+1515	00:35:14.9	15:15:04	13.73	LBL
1ES 0033+595	00:35:52.6	59:50:04	18.93	HBL
1ES 0037+405	00:40:13.8	40:50:04	16.8	HBL
RXS J0045.3+2127	00:45:19.1	21:27:43	16.89	HBL
B3 0045+395	00:47:55.2	39:48:57	–	–
EXO 0044.4+2001	00:47:08	20:17:44	16.05	IBL
PKS 0047+023	00:49:43.3	02:37:04	13.56	LBL
PKS 0048-097	00:50:41.2	–09:29:06	13.39	LBL
NPM1G -09.0033	00:56:20	–09:36:32	–	–
RXS J0058.2+1723	00:58:16.8	17:23:14	–	–
Q J0109+181	01:09:08.1	18:16:03	–	–
NPM1G +41.0022	01:10:04.8	41:49:50	17.7	HBL
RXS J0111.5+0536	01:11:30.1	05:36:28	–	–
S2 0109+22	01:12:05.8	22:44:39	13.59	LBL
RXS J0115.7+2519	01:15:46.5	25:19:57	13.43	LBL
1ES 0120+340	01:23:08.7	34:20:51	18.32	HBL
MS 0122.1+0903	01:24:44.5	09:18:49	15.53	IBL
B3 0133+388	01:36:32.6	39:06:00	16.59	HBL
PKS 0139-09	01:41:25.8	–09:28:43	13.4	LBL
1ES 0145+138	01:48:29.7	14:02:18	15.44	IBL
NPM1G +01.0067	01:52:39.6	01:47:17	–	–
8C 0149+710	01:53:25.8	71:15:07	14.75	IBL
RXS J0155.9+1502	01:56:00.3	15:02:13	–	–
87GB 01569+1032	01:59:34.4	10:47:07	15.56	IBL
RXS J0200.4+2712	02:00:29.5	27:12:36	–	–
MS 0158.5+0019	02:01:06.1	00:34:00	17.87	HBL
RXS J0202.4+0849	02:02:26.4	08:49:12	–	–
S5 0159+72	02:03:33.3	72:32:53	13.99	LBL
MS 0205.7+3509	02:08:38.2	35:23:13	15.22	IBL
87GB 02109+5130	02:14:17.9	51:44:52	17.69	HBL
RXS J0216.5+2314	02:16:32.1	23:14:47	–	–
Z 0214+083	02:17:17	08:37:03	15.23	IBL
S4 0218+35	02:21:05.4	35:56:15	–	–
3C 66A	02:22:39.6	43:02:08	15.63	IBL
RXS J0227.2+0201	02:27:16.6	02:01:58	–	–
1ES 0229+200	02:32:48.6	20:17:17	19.45	HBL
Q 0230+3429	02:33:20.3	34:42:54	15.84	IBL
AO 0235+164	02:38:38.8	16:36:59	13.57	LBL
S5 0238+71	02:43:31	71:20:18	16.3	IBL
NPM1G +10.0097	02:45:13.5	10:47:23	–	–
RXS J0250.6+1712	02:50:38	17:12:08	–	–
MS 0257.9+3429	03:01:03.8	34:41:01	13.28	LBL
4C 47.08	03:03:35.2	47:16:17	14.18	LBL
RXS J0303.5+0554	03:03:30.1	05:54:17	–	–
PKS 0306+102	03:09:03.6	10:29:16	12.94	LBL
VZw331	03:13:57.9	41:15:24	14.48	LBL
RXS J0314.0+2445	03:14:02.7	24:44:31	12.67	LBL

Table 3. continued.

Source	RA(J2000)	Dec(J2000)	$\log \nu_{\rm peak}$	Class
RXS J0314.3+0620	03:14:23.9	06:19:57	19.57	HBL
RXS J0316.1+0904	03:16:12.9	09:04:43	15.91	IBL
MS 03170+1834	03:19:51.8	18:45:35	16.99	HBL
RGB J0321+2336	03:22:00	23:36:11	–	–
2E 0323+0214	03:26:13.9	02:25:14	19.87	HBL
RXS J0331.3+0654	03:31:19.4	06:54:28	–	–
RXS J0349.9+0640	03:49:59.7	06:40:56	–	–
PKS 0406+121	04:09:22.1	12:17:39	13.22	LBL
2E 0414+0057	04:16:52.4	01:05:24	20.71	HBL
1WGA J0421.5+1433	04:21:33.1	14:33:54	13.93	LBL
MS 0419.3+1943	04:22:18.5	19:50:53	16.82	HBL
PKS 0420+022	04:22:52.2	02:19:27	–	–
PKS 0422+004	04:24:46.8	00:36:07	15.69	IBL
MCG 38364	04:25:51.3	–08:33:38	17.17	HBL
2EG J0432+2910	04:33:37.7	29:05:56	14.09	LBL
1ES 0446+449	04:50:07.3	45:03:12	–	–
PKS 0459+135	05:02:33.2	13:38:11	13.55	LBL
Q 0458+6530	05:03:03.4	65:34:10	18.12	HBL
RXS J0505.5+0416	05:05:34.7	04:15:54	16.94	HBL
1ES 0502+675	05:07:56.1	67:37:24	19.18	HBL
S5 0454+84	05:08:42.5	84:32:05	13.58	LBL
MG 0509+0541	05:09:25.9	05:41:35	15.34	IBL
4U 0506-03	05:09:39	–04:00:36	17.94	HBL
2E 0514+0626	05:17:04	06:29:39	–	–
1ES 0525+713	05:31:41.7	71:22:17	–	–
TEX 0554+534	05:58:11.6	53:28:19	14.44	LBL
MS 0607.9+7108	06:13:42.8	71:07:29	14.85	IBL
87GB 06216+4441	06:25:18.3	44:40:02	13.61	LBL
1ES 0647+250	06:50:46.5	25:03:00	18.28	HBL
B3 0651+428	06:54:43.5	42:47:59	15.12	IBL
NPM1G +42.0131	06:56:10.6	42:37:02	17.25	HBL
EXO 0706.1+5913	07:10:30.1	59:08:21	21.05	HBL
RXS J0712.3+5719	07:12:18.7	57:19:22	–	–
S5 0716+714	07:21:53.3	71:20:36	14.46	LBL
RXS J0723.2+5841	07:23:13.2	58:41:23	–	–
FIRST J0724.7+2621	07:24:42.8	26:21:30	16.39	IBL
PKS 0723-008	07:25:50.7	–00:54:56	–	–
FIRST J0730.4+3307	07:30:26.1	33:07:22	16.29	IBL
RXS J0737.3+3517	07:37:21	35:17:41	17.77	HBL
FIRST J0738.6+3139	07:38:37.8	31:39:30	–	–
PKS 0735+17	07:38:07.4	17:42:19	13.95	LBL
FIRST J0741.3+2253	07:41:18.8	22:53:39	–	–
MS 0737.9+7441	07:44:05.1	74:33:59	13.61	LBL
S4 0749+54	07:53:01.3	53:53:00	13.12	LBL
GB 0751+485	07:54:45.7	48:23:51	14.32	LBL
PKS 0754+100	07:57:06.7	09:56:35	13.63	LBL
RXS J0800.1+6210	08:00:06.5	62:10:12	–	–
RXS J0801.0+6444	08:01:00.7	64:44:43	–	–
RXS J0805.4+7534	08:05:26.5	75:34:25	15.96	IBL
SBS 0802+596	08:06:25.9	59:31:07	16.69	HBL
B2 0806+31	08:09:13.4	31:22:22	–	–
RXS J0809.6+3455	08:09:38.5	34:55:37	18.29	HBL
1ES 0806+524	08:09:49.2	52:18:58	16.56	HBL
PKS 0808+019	08:11:26.6	01:46:52	13.17	LBL
RXS J0812.1+5717	08:12:08.8	57:17:34	–	–

Table 3. continued.

Source	RA(J2000)	Dec(J2000)	$\log \nu_{\rm peak}$	Class
EXO 0811.2+2949	08:14:21.8	29:40:32	–	–
1WGA J0816.0-0736	08:16:04.3	–07:35:57	14.19	LBL
RXS J0816.3+5739	08:16:23.8	57:39:03	17.19	HBL
RXS J0816.6+6208	08:16:40.9	62:08:44	15.25	IBL
OJ 425	08:18:16.1	42:22:46	13.33	LBL
FIRST J0818.4+2814	08:18:27.3	28:14:02	16.01	IBL
FIRST J0819.4+4037	08:19:25.8	40:37:43	16.61	HBL
FIRST J0820.3+3640	08:20:20.2	36:40:04	14	LBL
4C 22.21	08:23:24.8	22:23:03	13.09	LBL
PKS 0823+033	08:25:50.3	03:09:24	13.08	LBL
RXS J0828.2+4153	08:28:14.2	41:53:50	18.66	HBL
B3 0827+395	08:30:19.4	39:23:47	–	–
PKS 0829+046	08:31:48.9	04:29:39	13.53	LBL
1H 0827+089	08:31:54.8	08:47:58	14.22	LBL
OJ 448	08:32:23.2	49:13:21	13.06	LBL
TEX 0836+182	08:39:30.7	18:02:47	14.55	IBL
FIRST J0847.0+4117	08:47:02.5	41:17:57	18.11	HBL
RXS J0847.2+1133	08:47:12.9	11:33:52	19.13	HBL
RXS J0848.4+8111	08:48:27.8	81:11:47	–	–
US 1889	08:54:09.9	44:08:31	17.42	HBL
OJ 287	08:54:48.8	20:06:30	13.89	LBL
NPM1G -09.0307	09:08:02.2	–09:59:37	15.52	IBL
B2 0906+31	09:09:53.3	31:06:03	17.4	HBL
Ton 1015	09:10:37.1	33:29:24	15.39	IBL
FIRST J0910.8+3902	09:10:52	39:02:02	18.33	HBL
B2 0912+29	09:15:52.4	29:33:24	16	IBL
RXS J0916.8+5238	09:16:52	52:38:28	17.22	HBL
MS 0922.9+7459	09:28:02.6	74:47:19	–	–
RXS J0929.2+5013	09:29:15.4	50:13:35	14.59	IBL
S5 0916+86	09:29:42.7	86:12:21	14.16	LBL
1ES 0927+500	09:30:37.5	49:50:25	21.13	HBL
B2 0927+35	09:30:55.3	35:03:38	14.8	IBL
RXS J0930.9+3933	09:30:56.8	39:33:33	–	–
SBS 0936+522	09:39:37.9	52:01:46	–	–
B2 0937+26	09:40:13.6	26:03:26	14.75	IBL
US 1015	09:50:11.8	45:53:20	15.48	IBL
RGB J0952+656	09:52:32.2	65:38:01	15.08	IBL
MS 0950.9+4929	09:54:09.8	49:15:00	16.92	HBL
S4 0954+65	09:58:47.2	65:33:54	13.76	LBL
4C 22.25	10:00:21.36	22:33:07.4	–	–
MS 0958.9+2102	10:01:42.4	20:48:18	15.54	IBL
EXO 1004.0+3509	10:06:56.3	34:54:45	16.92	HBL
RXS J10081+4705	10:08:11.3	47:05:20	19.67	HBL
NRAO 350	10:12:13.3	06:30:57	16.09	IBL
RXS J1012.7+4229	10:12:44.3	42:29:57	20.97	HBL
GB 1011+496	10:15:04.2	49:26:01	16.74	HBL
RXS J1016.2+4108	10:16:16.7	41:08:13	16.62	HBL
RXS J1022.7-0112	10:22:43.9	–01:12:56	17.97	HBL
1ES 1028+511	10:31:18.5	50:53:36	18.56	HBL
FIRST J1032.6+3738	10:32:40.7	37:38:26	–	–
RXS J1037.7+5711	10:37:44.2	57:11:57	14.95	IBL
TEX 1040+244	10:43:09	24:08:35	13.1	LBL
1ES 1044+549	10:47:45.8	54:37:41	13	LBL
MS 1050.7+4946	10:53:44.2	49:29:54	15.29	IBL
FIRST J1054.5+3855	10:54:31.8	38:55:22	16.68	HBL

Table 3. continued.

Source	RA(J2000)	Dec(J2000)	$\log \nu_{\rm peak}$	Class
RXS J1055.5-0126	10:55:34.1	–01:26:05	–	–
RXS J1056.1+0252	10:56:06.6	02:52:13	–	–
FIRST J1057.3+2303	10:57:23.1	23:03:18	18.7	HBL
RXS J1057.8+0059	10:57:52.4	00:59:13	–	–
FIRST J1058.4+2817	10:58:29.9	28:17:46	18.37	HBL
RXS J1058.6+5628	10:58:37.7	56:28:12	15.64	IBL
MC 1057+100	11:00:20.2	09:49:35	–	–
RXS J1100.3+4019	11:00:21.1	40:19:28	18.76	HBL
RXS J1102.8-0148	11:02:52	–01:48:51	–	–
MRK 421	11:04:27.2	38:12:32	18.49	HBL
1ES 1106+244	11:09:16.2	24:11:20	16.91	HBL
OP 1106.7+3654	11:09:33.5	36:38:26	–	–
FIRST J1110.9+3539	11:10:56.9	35:39:06	–	–
RXS J1110.6+7133	11:10:37.5	71:33:57	16.96	HBL
RXS J1111.5+3452	11:11:30.9	34:52:00	–	–
FIRST J1117.6+2548	11:17:40.4	25:48:46	15.71	IBL
EXO 1118.0+4228	11:20:48.1	42:12:13	17.41	HBL
US 2504	11:29:50.1	26:52:53	12.97	LBL
MS 1133.7+1618	11:36:17.6	16:01:53	15.9	IBL
MRK 180	11:36:26.5	70:09:28	18.61	HBL
RXS J1136.5+6737	11:36:30.1	67:37:04	17.55	HBL
FIRST J1136.8+2550	11:36:50.1	25:50:52	15.13	IBL
2E 1146+2456	11:49:29.9	24:38:55	17.87	HBL
EXO 1449.9+2455	11:49:30.3	24:39:27	19.83	HBL
B2 1147+245	11:50:19.2	24:17:54	13.95	LBL
RXS J1151.4+5859	11:51:24.6	58:59:14	16.4	IBL
FIRST J1152.1+2837	11:52:10.7	28:37:21	14.8	IBL
FIRST J1153.7+3823	11:53:42.9	38:23:06	–	–
MS 1154.1+4255	11:56:46.6	42:38:10	14.91	IBL
B3 1159+450	12:02:08.6	44:44:21	15.92	IBL
B3 1206+416	12:09:22.8	41:19:41	14.59	IBL
1207+39W4	12:10:26.6	39:29:08	–	–
MS 1209.0+3917	12:11:34.2	39:00:55	–	–
1ES 1212+078	12:15:10.9	07:32:03	15.91	IBL
Q 1214+1753	12:16:56.9	17:37:12	–	–
B2 1215+30	12:17:52	30:07:01	15.58	IBL
GB2 1217+348	12:20:08.4	34:31:22	14.46	LBL
PG 1218+304	12:21:21.9	30:10:37	19.14	HBL
ON 231	12:21:31.7	28:13:58	14.84	IBL
UM 493	12:22:06.5	–01:06:38	–	–
RXS J1222.2+3541	12:22:12.4	35:41:00	12.81	LBL
S5 1221+80	12:23:40.4	80:40:04	14.21	LBL
MS 1221.8+2452	12:24:24.3	24:36:24	13.99	LBL
1WGA J1225.3+1818	12:25:18.2	18:18:20	14.71	IBL
FIRST J1226.0+2604	12:26:04.1	26:04:28	16.29	IBL
RXS J1230.2+2517	12:30:14	25:18:06	14.9	IBL
2E 1258+1437	12:31:23.9	14:21:25	14.91	IBL
MS 1229.2+6430	12:31:31.3	64:14:18	16.25	IBL
B2 1229+29	12:31:43.6	28:47:49	–	–
FIRST J1236.3+3900	12:36:23.1	39:00:01	16.61	HBL
MS 1235.4+6315	12:37:38.6	62:58:44	15.98	IBL
RXS J1237.0+3020	12:37:05.5	30:20:04	–	–
1ES 1239+069	12:41:48.3	06:36:01	17.38	HBL
RXS J1241.6+3440	12:41:41.2	34:40:32	–	–
Ton 116	12:43:12.7	36:27:44	–	–

Table 3. continued.

Source	RA(J2000)	Dec(J2000)	$\log \nu_{\rm peak}$	Class
PG 1246+586	12:48:18.8	58:20:29	15.05	IBL
1ES 1249+174E	12:51:45.5	17:11:17	–	–
FIRST J1252.3+2640	12:52:19.5	26:40:53	–	–
S4 1250+53	12:53:11.9	53:01:11	14.82	IBL
1ES 1255+244	12:57:31.9	24:12:40	16.89	HBL
MS 1256.3+0151	12:58:54.6	01:34:43	–	–
MS 1258.4+6401	13:00:17.6	63:44:39	16.35	IBL
FIRST J1301.7+4056	13:01:45.7	40:56:24	16.55	HBL
RXS J1302.9+5056	13:02:55.5	50:56:17	–	–
MC2 1307+12	13:09:33.9	11:54:24	13.07	LBL
1WGA J1309.6+0828	13:09:38.9	08:28:28	14.64	IBL
AUCVn	13:10:28.66	32:30:43.8	13.75	LBL
HS 1309+2605	13:12:19.2	25:49:58	–	–
TEX 1312+240	13:14:43.8	23:48:26	15.84	IBL
RXS J1319.5+1405	13:19:31.7	14:05:34	20.85	HBL
UM 566	13:19:55.1	01:52:58	–	–
1ES 1320+084N	13:22:54.9	08:10:10	13.12	LBL
RXS J1324.0+5739	13:24:00.8	57:39:16	15.48	IBL
RXS J1326.2+2933	13:26:15	29:33:29	–	–
RXS J1326.2+1230	13:26:17.6	12:30:00	16.32	IBL
RX J1340.1+2743	13:40:10.9	27:43:48	–	–
RXS J1340.4+4410	13:40:29.8	44:10:04	16.51	HBL
RXS J1341.0+3959	13:41:05	39:59:45	20.06	HBL
1338.8+2705	13:41:05.8	26:50:26	–	–
1340.8+2721	13:43:05.1	27:06:24	–	–
RXS J1353.4+5601	13:53:28	56:00:55	19.23	HBL
FIRST J1354.4+3706	13:54:26.7	37:06:54	16.92	HBL
RXS J1359.8+5911	13:59:53.7	59:11:01	13.66	LBL
MC 1400+162	14:02:44.5	15:59:57	16.47	IBL
RXS J1404.8+6554	14:04:49.6	65:54:30	–	–
MS 1402.3+0416	14:04:51	04:02:02	15.83	IBL
MS 1407.9+5954	14:09:23.5	59:39:41	16.63	HBL
PKS 1407+022	14:10:04.6	02:03:07	13.69	LBL
RXS J1410.5+6100	14:10:31.7	61:00:10	20.25	HBL
FIRST J1414.1+3430	14:14:09.3	34:30:57	–	–
RGB J1415+485	14:15:36.8	48:30:30	14.56	IBL
PKS 1413+135	14:15:58.8	13:20:24	12.83	LBL
CRSS 1416.3+1137	14:16:20.7	11:37:37	–	–
2E 1415+2557	14:17:56.6	25:43:25	19.24	HBL
OQ 530	14:19:46.6	54:23:14	14.16	LBL
RXS J1422.6+5801	14:22:39	58:01:55	–	–
FIRST J1426.1+3404	14:26:07.7	34:04:26	14.1	LBL
PKS 1424+240	14:27:00.5	23:48:00	15.7	IBL
RGB J1427+541	14:27:30.3	54:09:24	14.89	IBL
H 1426+428	14:28:32.7	42:40:21	18.55	HBL
TEX 1428+370	14:30:40.6	36:49:03	14.26	LBL
CSO 474	14:36:45.7	35:57:01	–	–
RXS J1436.9+5639	14:36:57.8	56:39:25	17.5	HBL
PG 1437+398	14:39:17.5	39:32:43	16.7	HBL
1ES 1440+122	14:42:48.3	12:00:40	16.45	IBL
MS 1443.5+6349	14:44:34.9	63:36:06	17.05	HBL
RXS J1445.0-0326	14:45:06.2	–03:26:12	–	–
RXS J1448.0+3608	14:48:00.6	36:08:31	16.73	HBL
RXS J1449.5+2746	14:49:32.8	27:46:21	18.82	HBL
RXS J1451 4+6354	14:51:27.5	63:54:19	–	–

Table 3. continued.

Source	RA(J2000)	Dec(J2000)	$\log \nu_{\rm peak}$	Class
SBS 1452+516	14:54:27.1	51:24:33	–	–
RXS J1456.0+5048	14:56:03.7	50:48:25	19.94	HBL
RXS J1458.4+4832	14:58:28	48:32:40	21.46	HBL
B3 1456+375	14:58:44.8	37:20:22	13.47	LBL
MS 1458.8+2249	15:01:01.9	22:38:06	15.26	IBL
FIRST J1502.1+2528	15:02:08.3	25:28:45	14.17	LBL
FIRST J1502.5+3350	15:02:34	33:50:55	13.66	LBL
RXS J1508.7+2709	15:08:42.9	27:09:10	17.3	HBL
SBS 1508+561	15:09:48	55:56:17	15.22	IBL
FIRST J1515.9+2426	15:15:56.2	24:26:20	15.89	IBL
RXS J1516.7+2918	15:16:41.6	29:18:10	18.62	HBL
PKS 1514+197	15:16:56.8	19:32:12	13.6	LBL
1H 1515+660	15:17:47.6	65:25:24	18.11	HBL
FIRST J1530.7+2310	15:30:44	23:10:13	–	–
FAQS J1530.7+5329	15:30:44.5	53:29:28	16.88	HBL
RXS J1532.0+3016	15:32:02.2	30:16:29	17.05	HBL
RXS J1533.4+3416	15:33:24.3	34:16:41	18.32	HBL
RGB J1534+372	15:34:47.2	37:15:55	14.26	LBL
1ES 1533+535	15:35:00.8	53:20:37	19.68	HBL
FIRST J1535.4+3922	15:35:29.1	39:22:46	16.38	IBL
MS 1534.2+0148	15:36:46.8	01:37:59	18.83	HBL
1ES 1544+820	15:40:15.8	81:55:07	17.79	HBL
4C 14.6	15:40:46.5	14:47:45.9	14.85	IBL
RXS J1542.9+6129	15:42:56.9	61:29:56	14.72	IBL
RXS J1544.3+0458	15:44:18.7	04:58:24	16.77	HBL
MS 1552.1+2020	15:54:24.1	20:11:25	17.12	HBL
PG 1553+11	15:55:43.1	11:11:24	16.49	IBL
MYC 1557+566	15:58:48.5	56:25:14	–	–
RXS J1602.2+3050	16:02:18	30:51:09	16.42	IBL
PKS 1604+159	16:07:06.4	15:51:34	14.73	IBL
RXS J1610.0+6710	16:10:04.1	67:10:26	17.45	HBL
B3 1615+412	16:17:06.6	41:06:45	14.41	LBL
87GB 16166+2206	16:18:47.9	21:59:26	15.66	IBL
4C 37.46	16:21:11.3	37:46:04.9	–	–
RXJ 1624.7+3726	16:24:43.4	37:26:42	–	–
RXS J1624.9+7554	16:24:56.5	75:54:55	13.3	LBL
RXS J1626.4+3513	16:26:25.6	35:13:38	15.28	IBL
RXS J1631.3+4217	16:31:24.7	42:17:03	18.99	HBL
RXS J1638.0+7326	16:38:02.6	73:26:10	–	–
RXS J1644.2+4546	16:44:20	45:46:44	17.48	HBL
1643.2+4021	16:44:53.2	40:16:28	–	–
FIRST J1645.9+2947	16:45:57.7	29:47:30	–	–
FIRST J1651.1+4212	16:51:09.2	42:12:53	17.82	HBL
RXS J1651.6+7218	16:51:41.5	72:18:19	–	–
RGB J1652+403	16:52:50	40:23:10	14.97	IBL
MRK 501	16:53:52.2	39:45:36	16.84	HBL
B3 1659+399	17:01:24.6	39:54:36	13.41	LBL
FIRST J1702.1+2643	17:02:09.6	26:43:15	14.27	LBL
FIRST J1702.6+3115	17:02:38.6	31:15:43	13.49	LBL
RXS J1704.8+7138	17:04:46.9	71:38:18	15.58	IBL
MS 1704.9+6046	17:05:34.9	60:42:17	17.17	HBL
FIRST J1712.8+2931	17:12:48.8	29:31:17	18.79	HBL
RXS J1718.6+7358	17:18:40.1	73:58:15	–	–
PKS 1717+177	17:19:13.1	17:45:07	13.08	LBL
RXS J1719.6+7443	17:19:41	74:43:00	14.19	LBL

Table 3. continued.

Source	RA(J2000)	Dec(J2000)	$\log \nu_{\rm peak}$	Class
B2 1722+40	17:24:05.5	40:04:38	13	LBL
H 1722+119	17:25:04.4	11:52:16	15.8	IBL
IZw187	17:28:18.6	50:13:11	17.42	HBL
RXS J1728.6+7041	17:28:38.3	70:41:08	13.6	LBL
RXS J1732.0+6926	17:32:05.4	69:26:16	–	–
OT 465	17:39:57.1	47:37:59	13.91	LBL
RGBJ 1742+597	17:42:32	59:45:06	14.18	LBL
NPM1G +19.0510	17:43:57.9	19:35:09	17.91	HBL
B3 1743+398B	17:45:37.7	39:51:31	17.71	HBL
1ES 1745+504	17:46:32.3	50:28:09	–	–
B3 1746+470	17:47:26.6	46:58:51	13.96	LBL
S4 1749+70	17:48:33.1	70:05:50	14.55	IBL
B3 1747+433	17:49:00.4	43:21:52	13.56	LBL
RXS J1750.0+4700	17:50:05	47:00:44	18.1	HBL
PKS 1749+096	17:51:32.7	09:39:01	12.78	LBL
RXS J1756.2+5522	17:56:15.9	55:22:18	19.9	HBL
MS 1757.7+7034	17:57:13.3	70:33:37	13.7	LBL
S5 1803+784	18:00:45.4	78:28:04	14.05	LBL
RX J1801.7+6638	18:01:46.7	66:38:40	–	–
3C 371	18:06:50.7	69:49:28	14.65	IBL
RGB J1808+468	18:08:01.2	46:49:41	14.63	IBL
RGB J1811+442	18:11:53.5	44:16:29	15.07	IBL
B2 1811+31	18:13:35.3	31:44:17	15.53	IBL
4C 56.27	18:24:07.07	56:51:01.5	12.95	LBL
RXS J1829.4+5402	18:29:24.3	54:03:00	15.07	IBL
Q 1832+6845	18:32:36.6	68:48:09	–	–
RXS J1838.7+4802	18:38:49.2	48:02:34	13.52	LBL
RGB J1841+591	18:41:20.3	59:06:08	14.91	IBL
RXS J1848.7+4245	18:48:47.1	42:45:39	–	–
1ES 1853+671	18:53:52.1	67:13:55	16.64	HBL
87GB 19021+5536	19:03:11.6	55:40:39	14.5	LBL
S4 1926+61	19:27:30.4	61:17:32	13.44	LBL
RXS J1931.1+0937	19:31:09.5	09:37:13	–	–
1ES 1959+650	19:59:59.9	65:08:55	18.03	HBL
S5 2007+77	20:05:31.1	77:52:43	13.15	LBL
S5 2010+72	20:09:52.3	72:29:19	13.64	LBL
PKS 2012-017	20:15:15.1	–01:37:33	14.68	IBL
S5 2023+76	20:22:35.6	76:11:26	14.1	LBL
PKS 2032+107	20:35:22.3	10:56:06	14	LBL
1ES 2037+521	20:39:23.5	52:19:50	16.13	IBL
PKS 2047+039	20:50:06.2	04:07:49	13.83	LBL
S5 2051+74	20:51:33.8	74:41:40	18.75	HBL
PKS 2131-021	21:34:10.2	–01:53:17	12.76	LBL
MS 2143.4+0704	21:45:52.3	07:19:27	13.92	LBL
PKS 2149+17	21:52:24.8	17:34:39	13.85	LBL
BL LAC	22:02:43.3	42:16:39	14.28	LBL
RXS J2209.3+1031	22:09:18.5	10:31:43	13.36	LBL
RXS J2219.7+2120	22:19:45.3	21:20:48	17.61	HBL
RXS J2225.1+1136	22:25:11.2	11:36:01	–	–
PKS 2223-114	22:25:43.7	–11:13:41	14.65	IBL
3C 446	22:25:45.1	–04:56:34	13.37	LBL
S5 2229+69	22:30:35.6	69:46:29	13.09	LBL
RXS J2233.0+1335	22:33:00.9	13:35:59	16.61	HBL
RGB J2243+203	22:43:54.7	20:21:04	14.15	LBL
B3 2247+381	22:50:05.8	38:24:37	15.61	IBL

Table 3. continued.

Source	RA(J2000)	Dec(J2000)	$\log \nu_{\rm peak}$	Class
PKS 2254+074	22:57:17.3	07:43:12	14.18	LBL
RXS J2304.6+3705	23:04:36.6	37:05:08	21.01	HBL
B3 2311+396A	23:13:50.2	40:03:03	–	–
Q J2319+161	23:19:43.4	16:11:51	15.48	IBL
TEX 2320+343	23:22:44	34:36:14	16.73	HBL
1ES 2321+419	23:23:54.1	42:11:19	13.26	LBL
B3 2322+396	23:25:17.9	39:57:37	15.29	IBL
1ES 2326+174	23:29:03.3	17:43:30	18.07	HBL
Q J2338+212	23:38:56.4	21:24:41	17.62	HBL
MS 2336.5+0517	23:39:07	05:34:36	14.91	IBL
1ES 2344+514	23:47:04.8	51:42:18	16.4	IBL
MS 2347.4+1924	23:50:01.7	19:41:52	15.8	IBL
RXS J2350.3-059	23:50:17.9	–05:59:28	–	–
TEX 2348+360	23:50:36.7	36:22:11	16.1	IBL
PKS 2354-02	23:57:25.1	–01:52:15	–	–

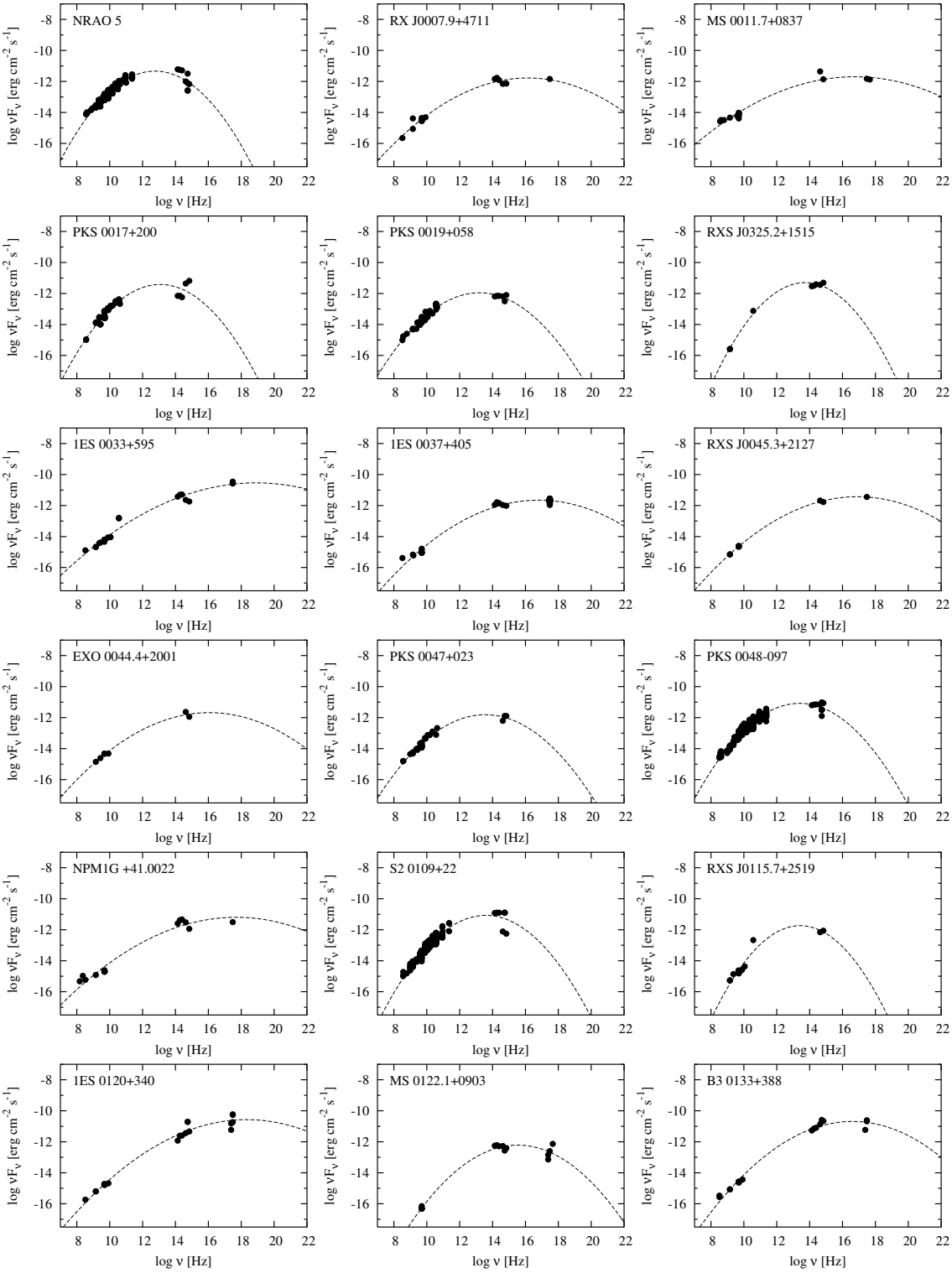

Fig. 13. Spectral energy distributions of the Metsähovi BL Lac sample. Only datapoints used in the fit are shown in the figure.

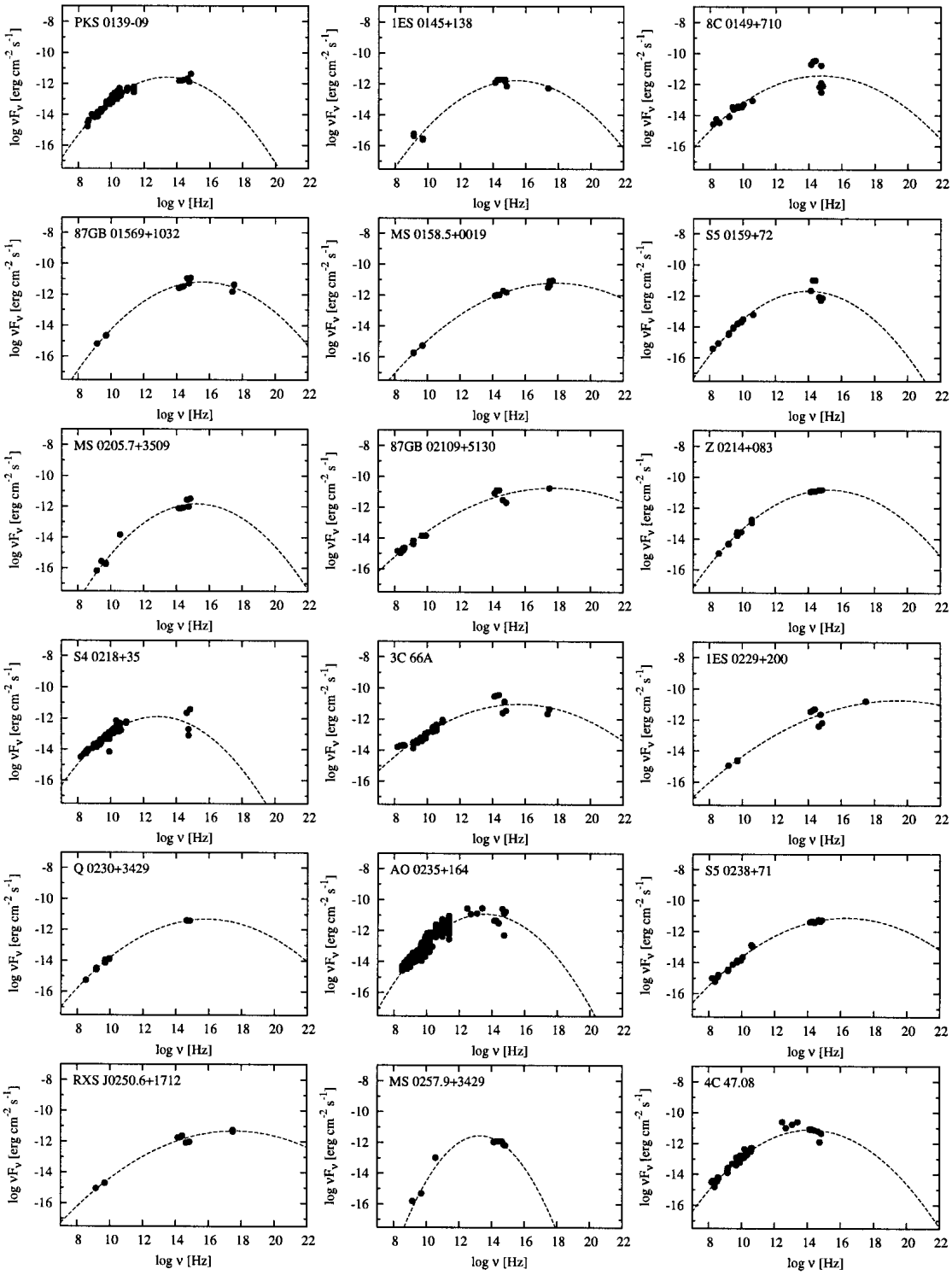

Fig. 13. continued.

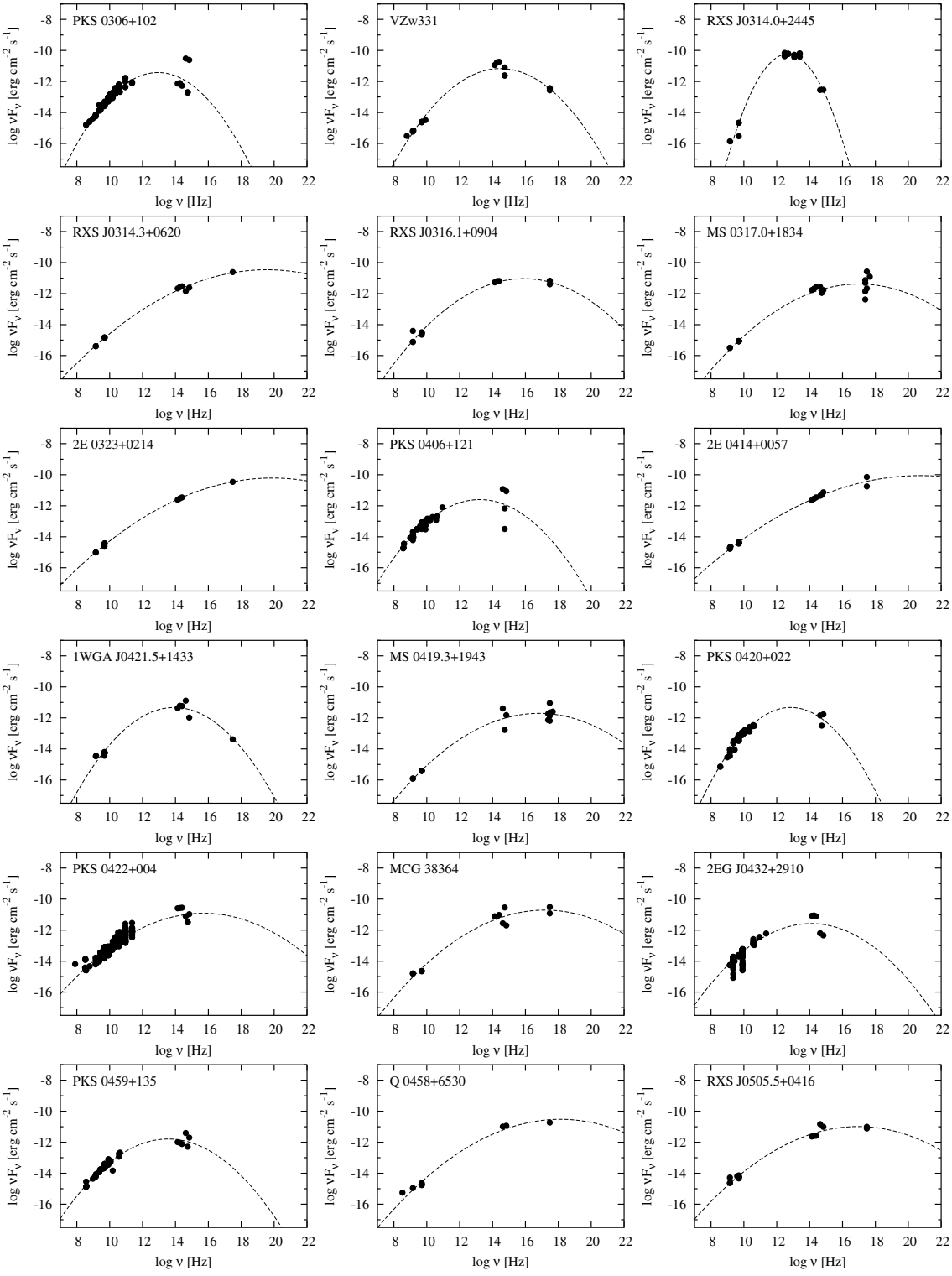

Fig. 13. continued.

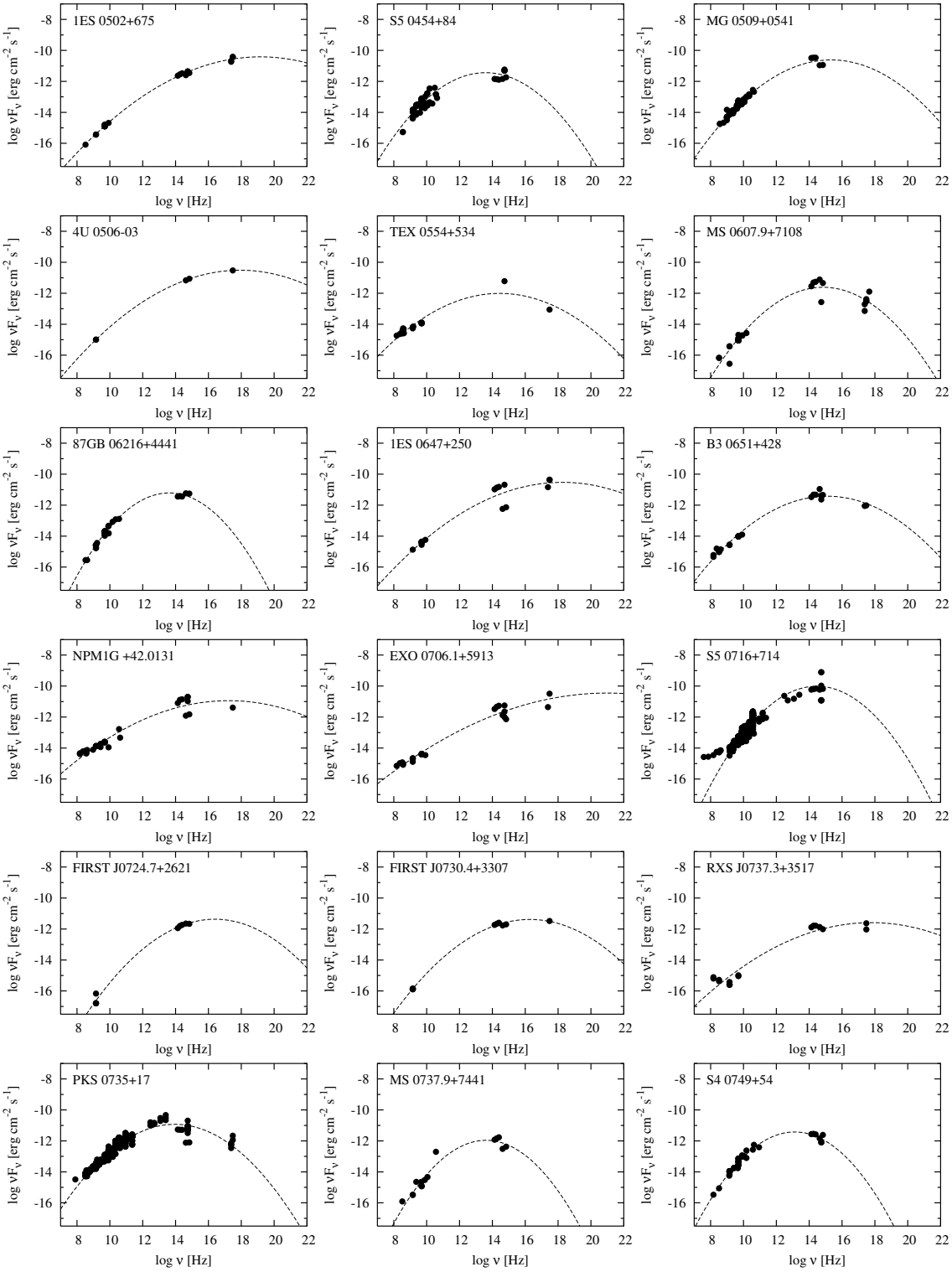

Fig. 13. continued.

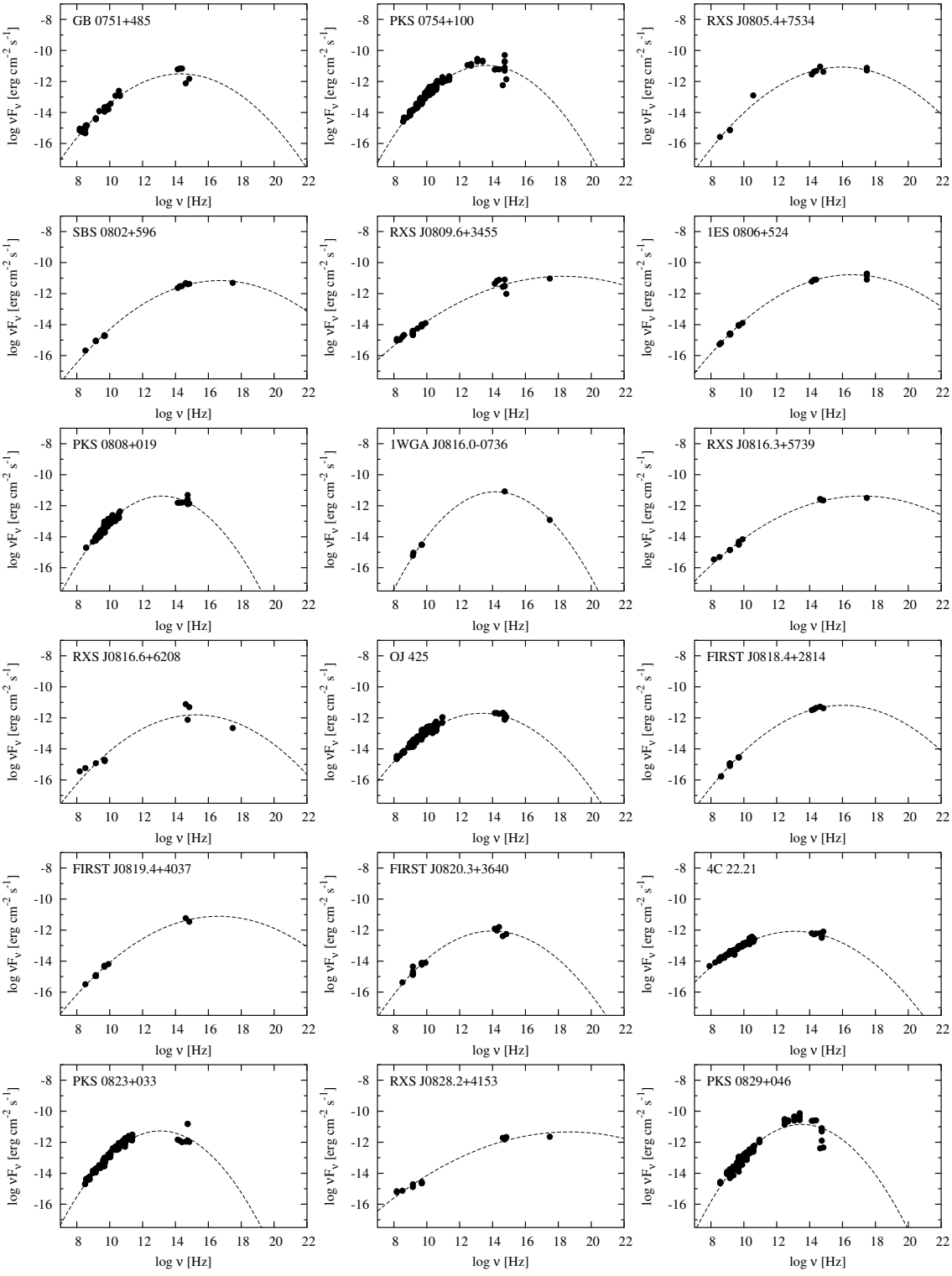

Fig. 13. continued.

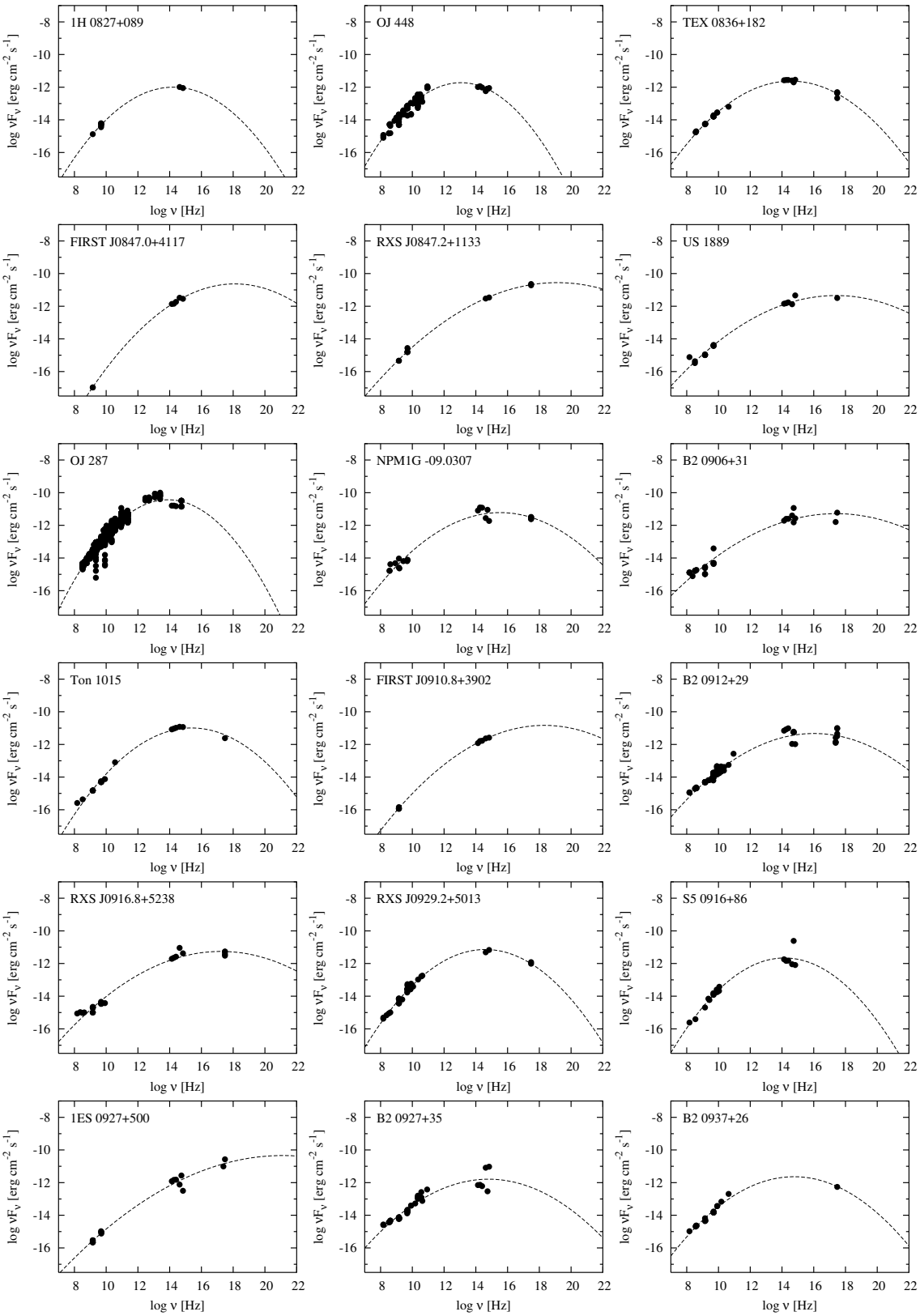

Fig. 13. continued.

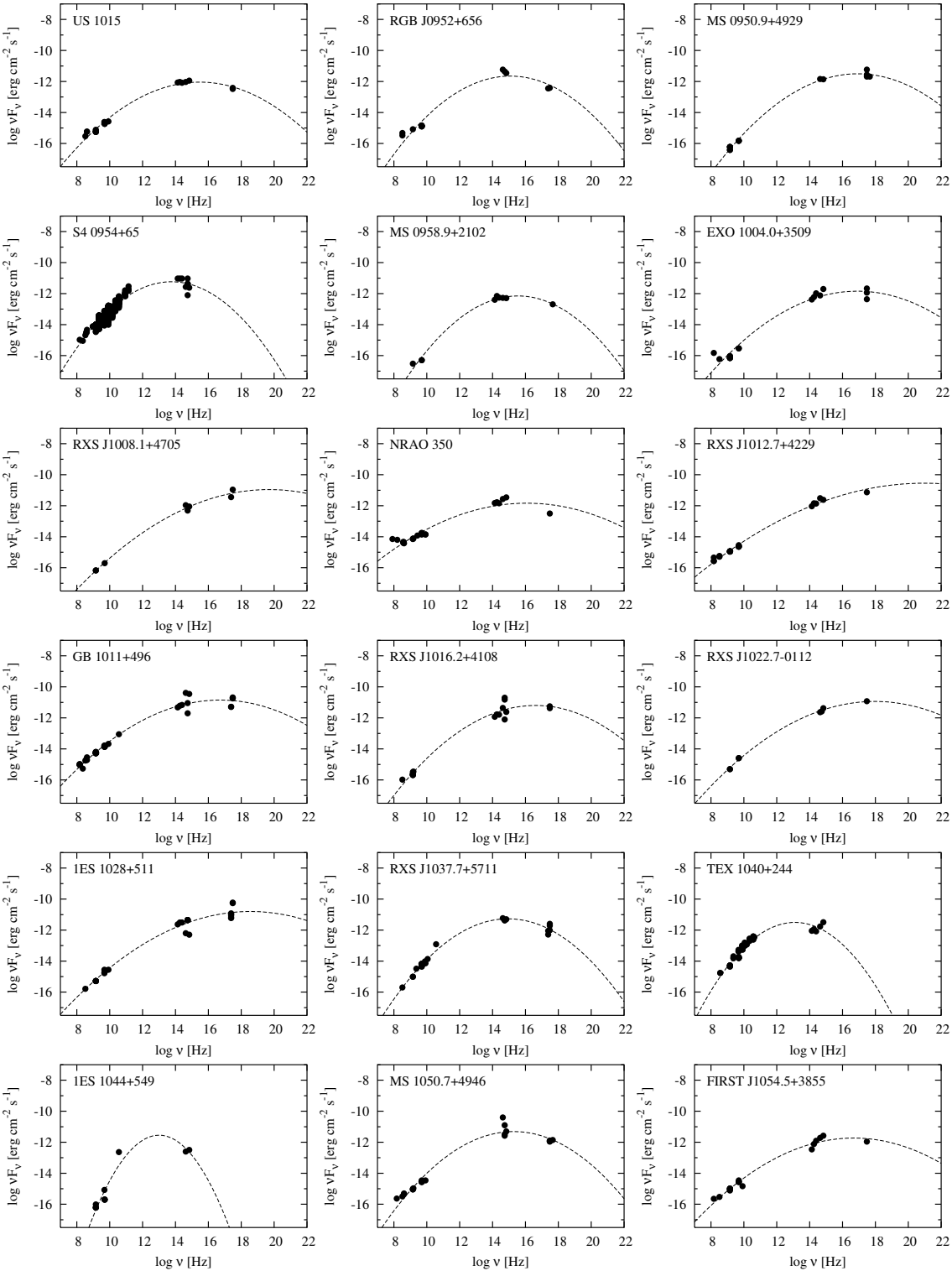

Fig. 13. continued.

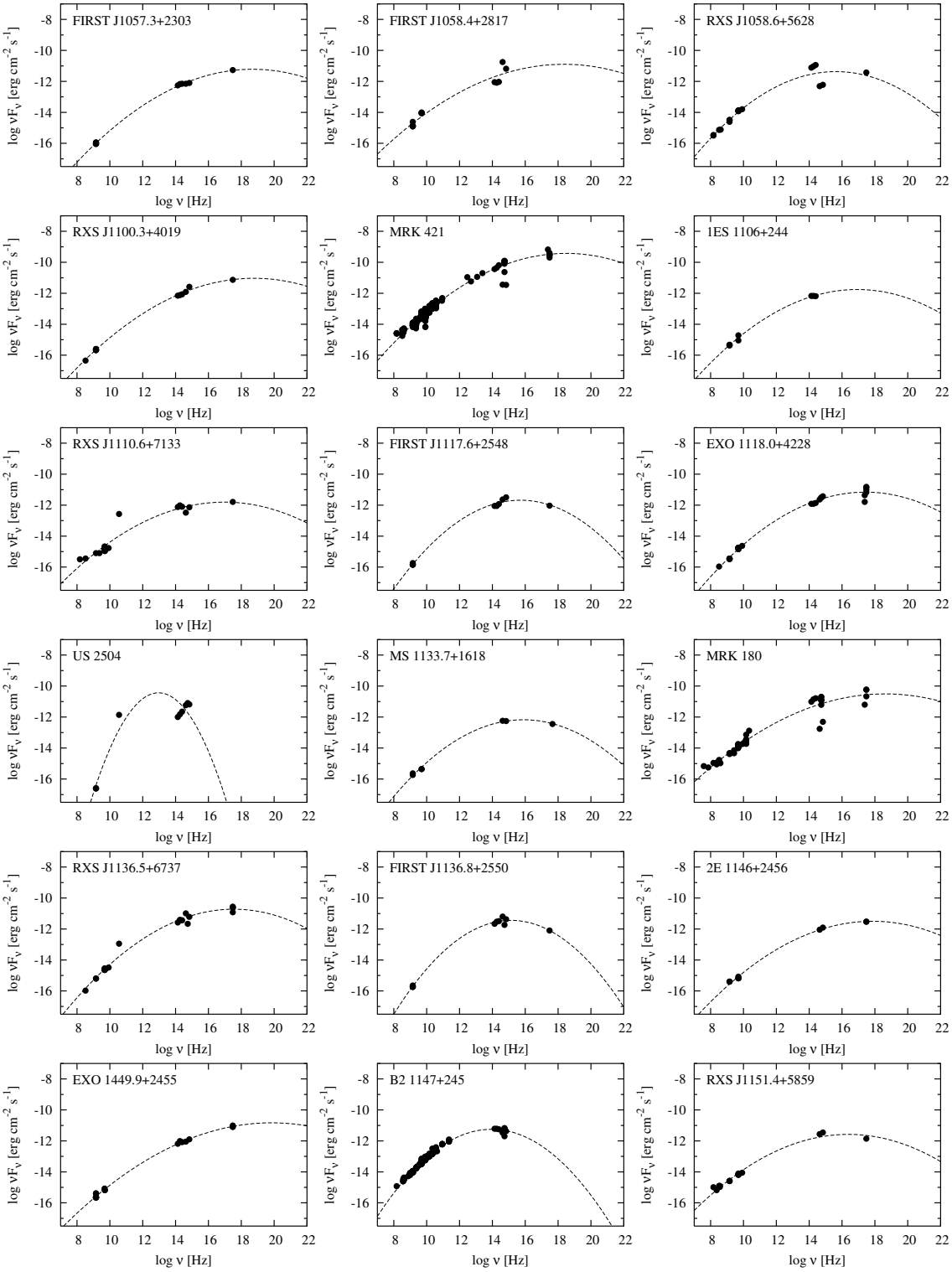

Fig. 13. continued.

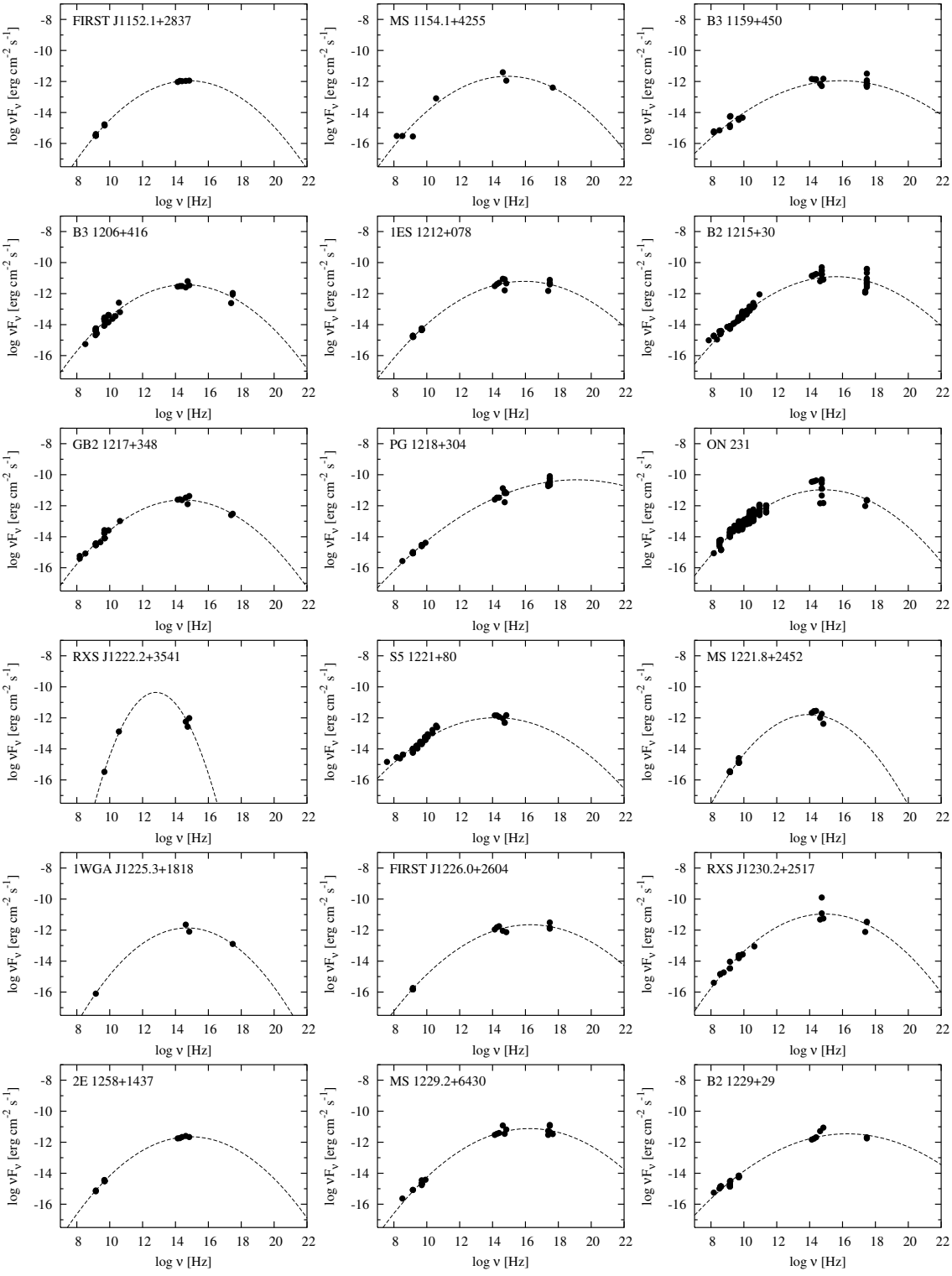

Fig. 13. continued.

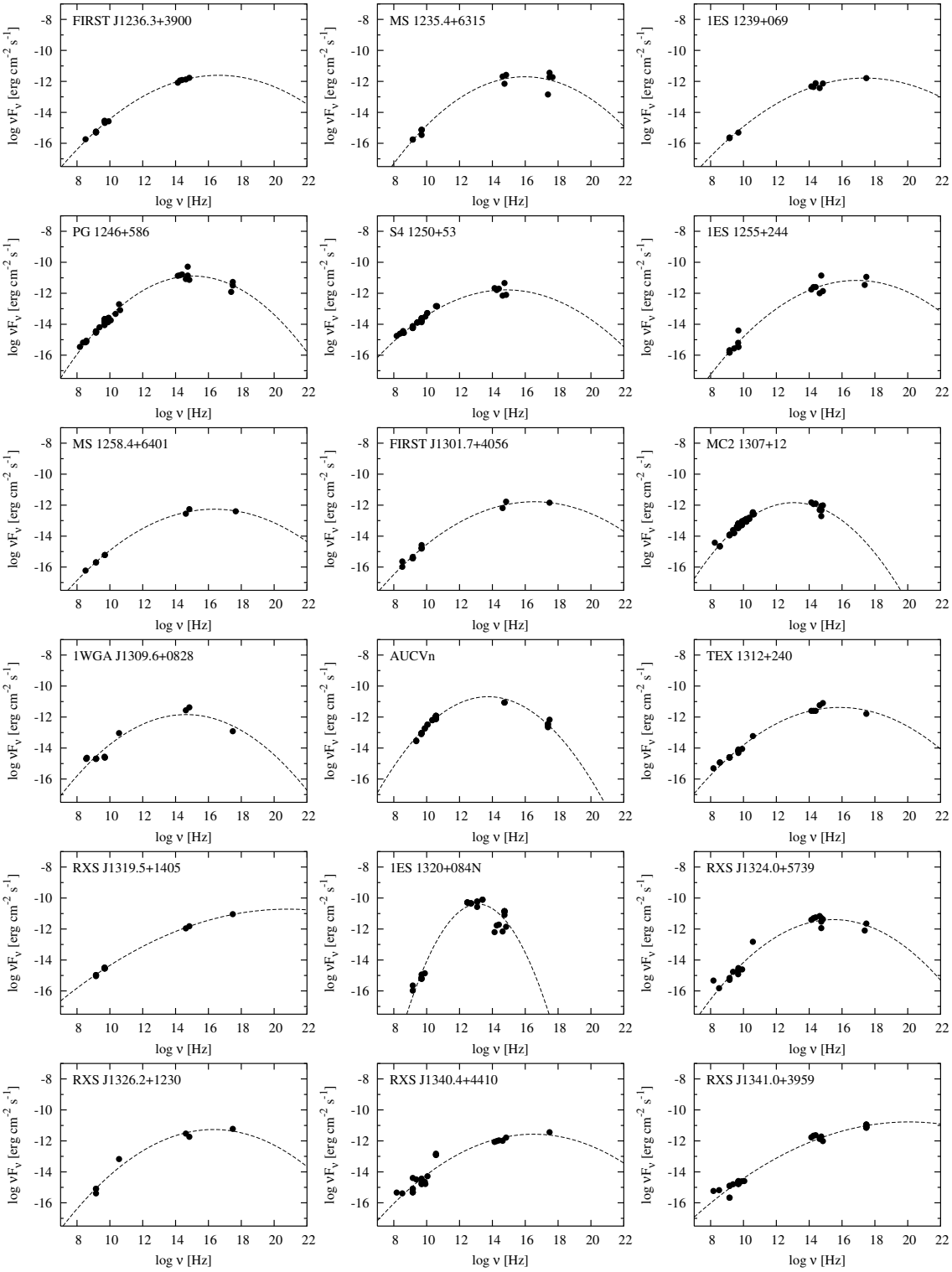

Fig. 13. continued.

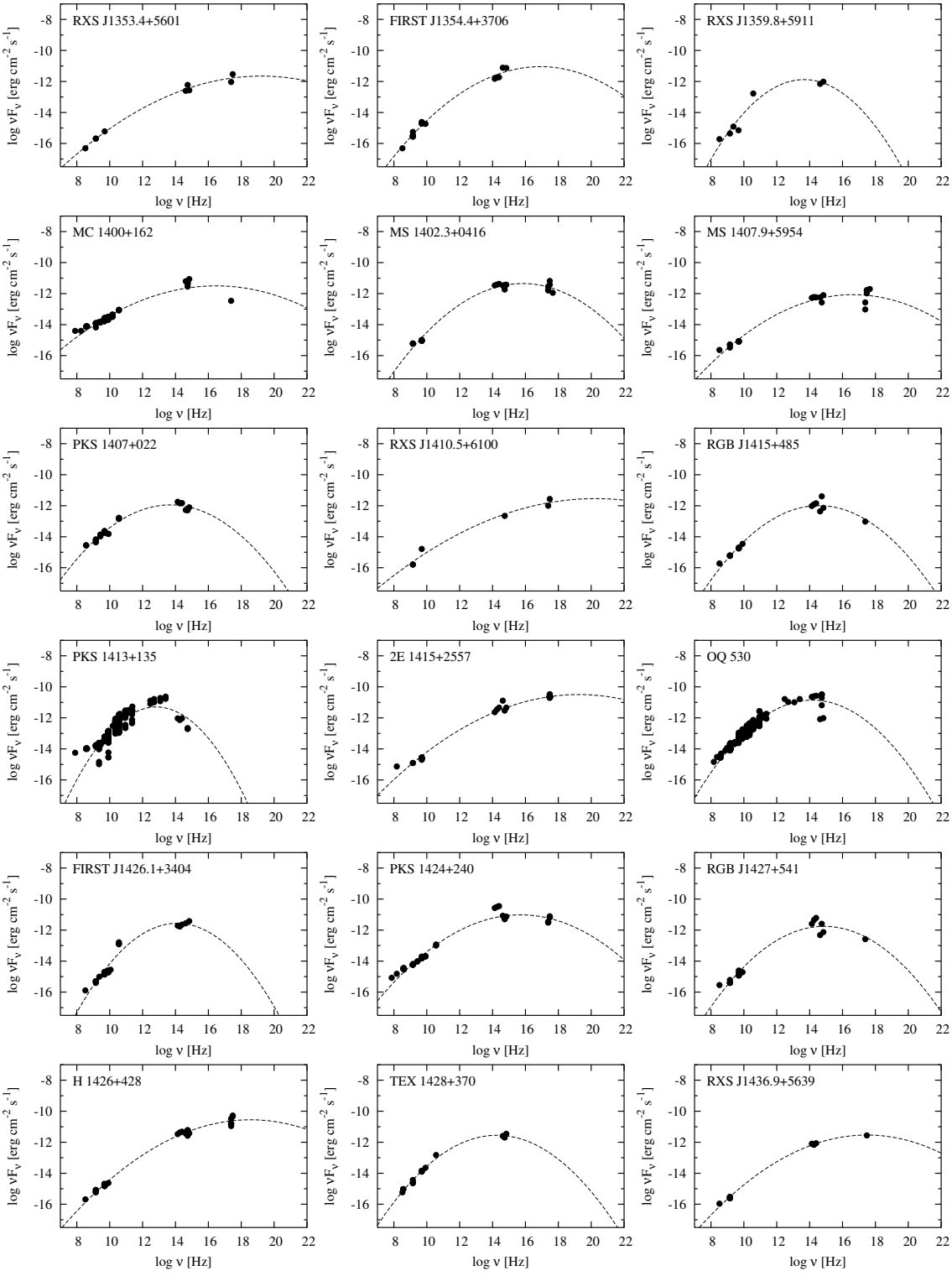

Fig. 13. continued.

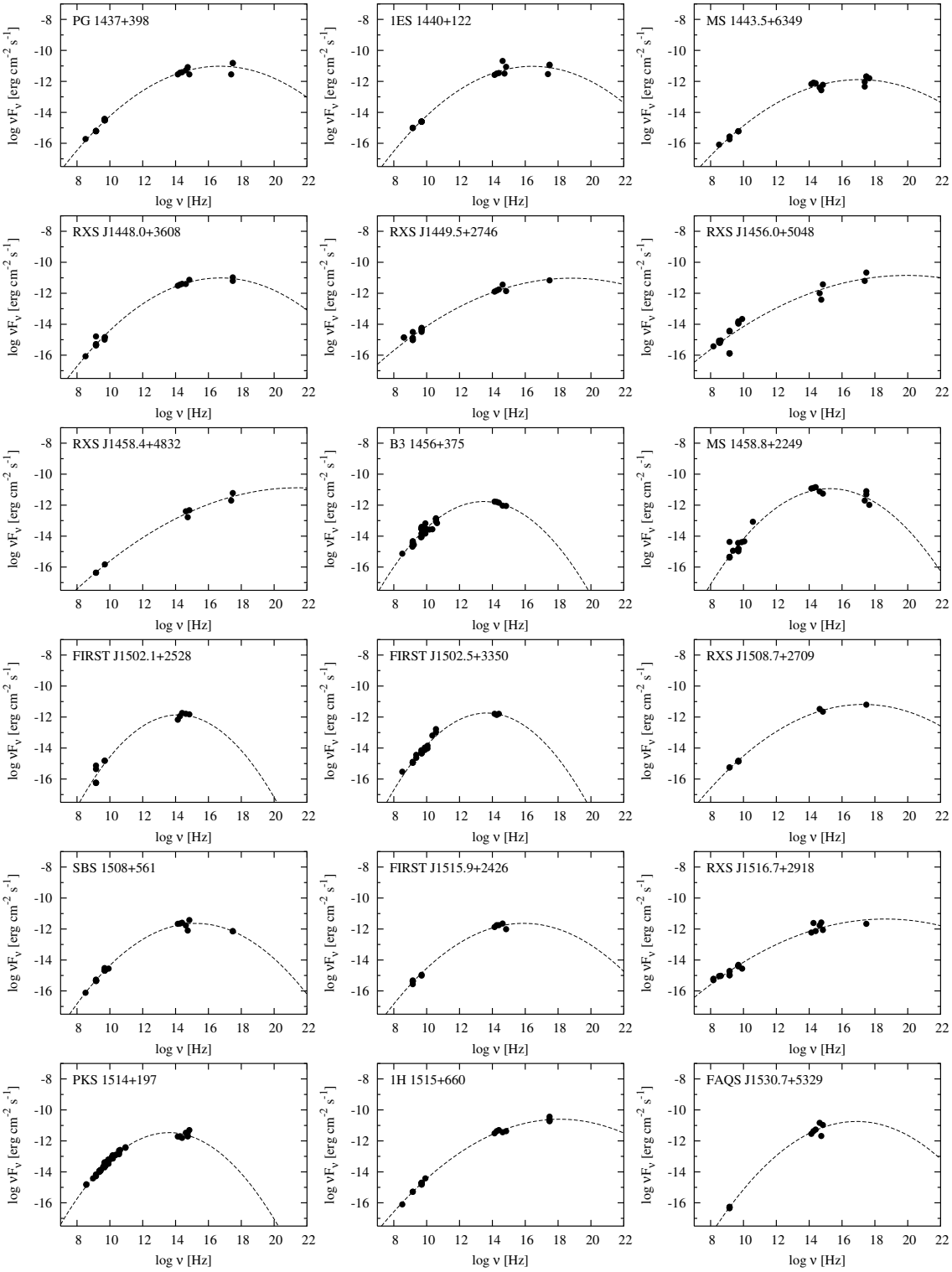

Fig. 13. continued.

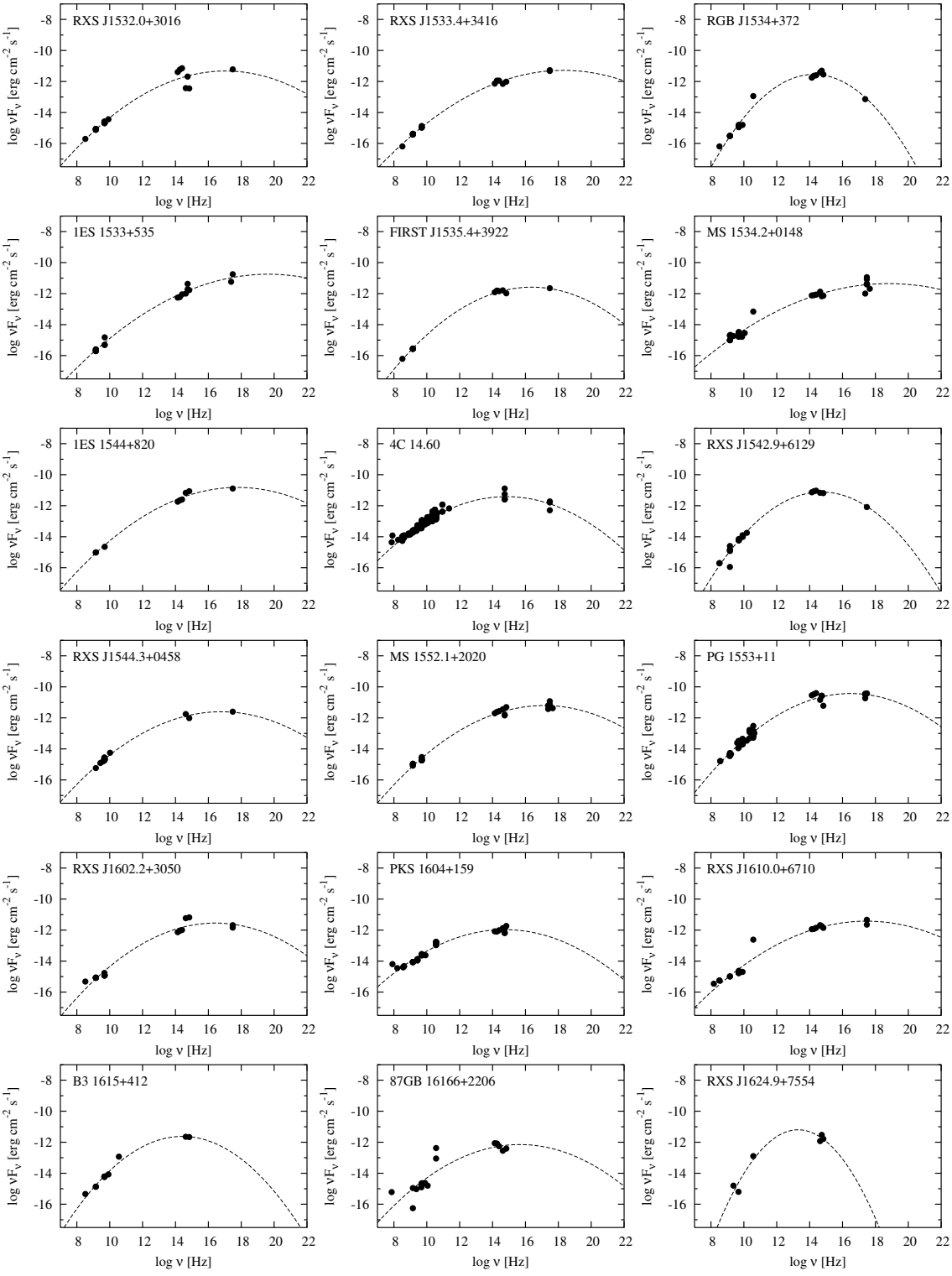

Fig. 13. continued.

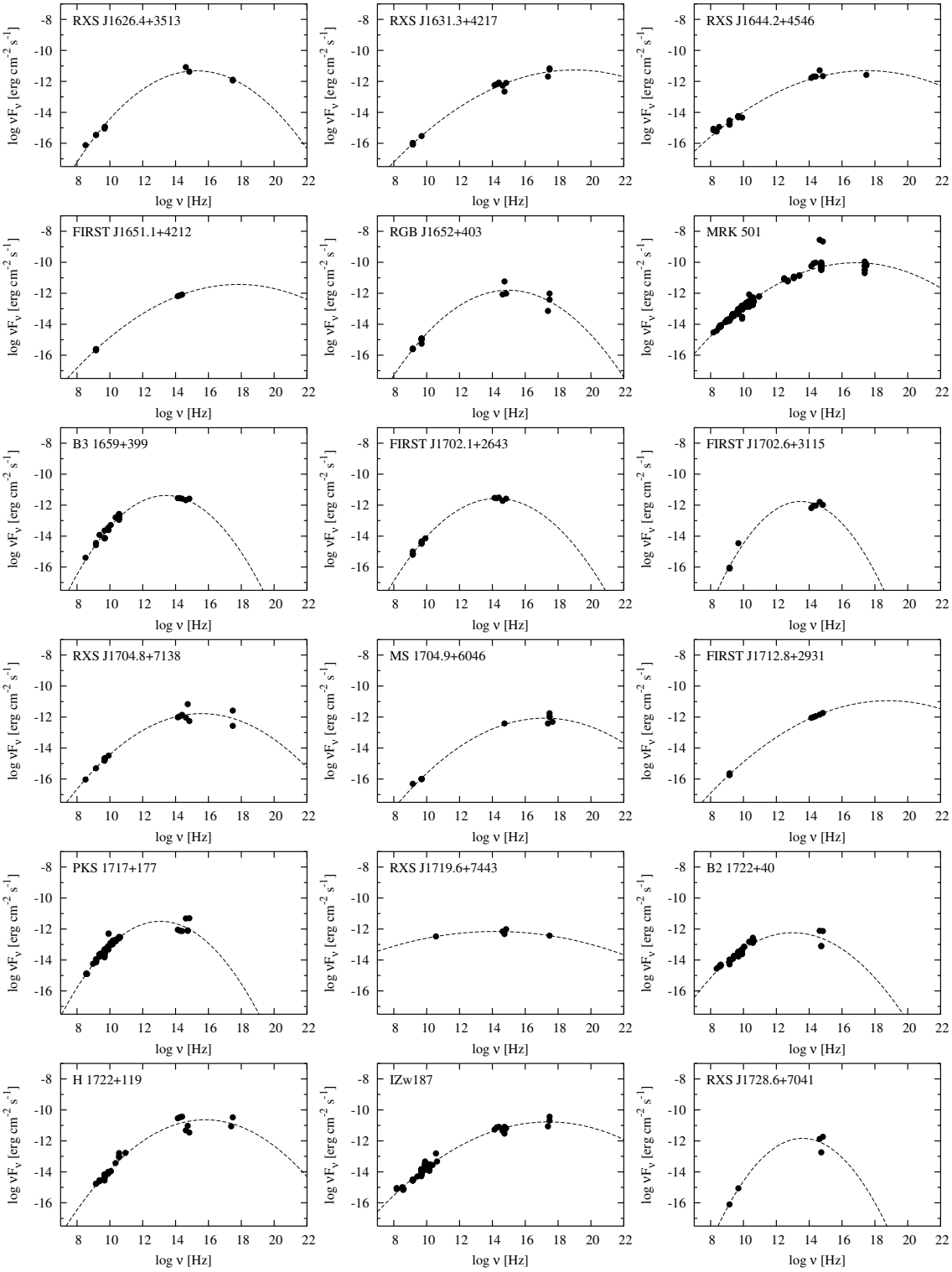

Fig. 13. continued.

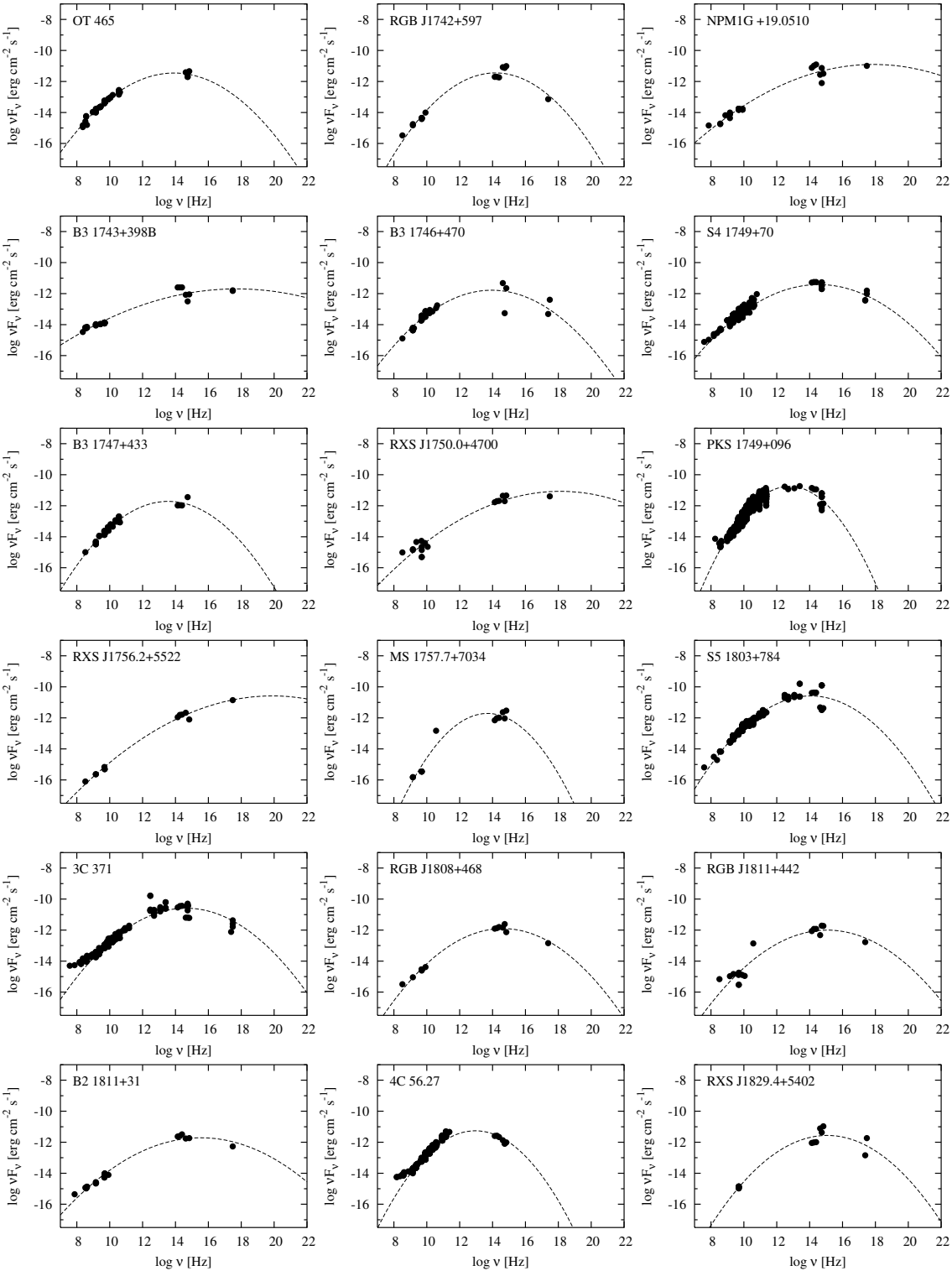

Fig. 13. continued.

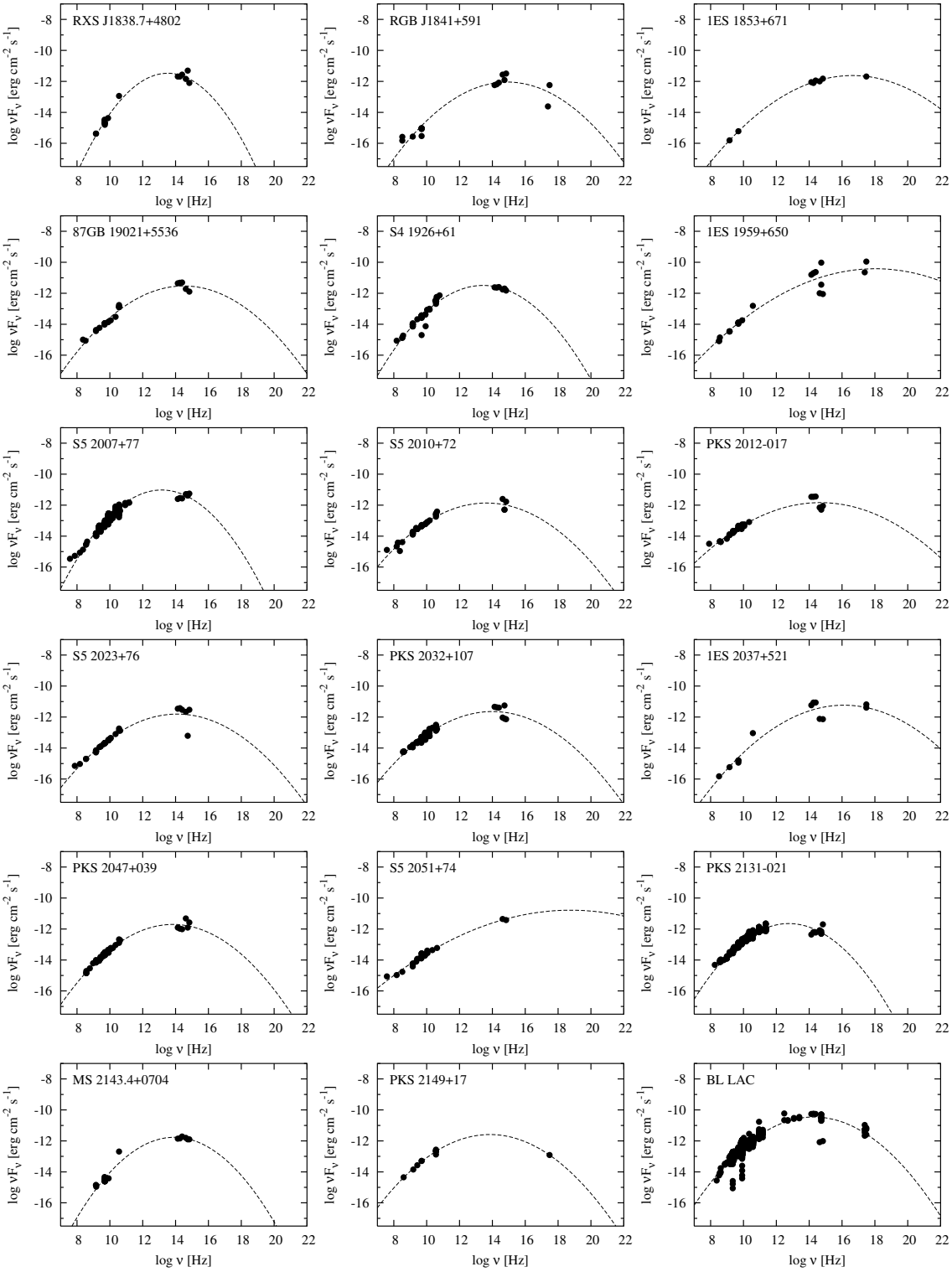

Fig. 13. continued.

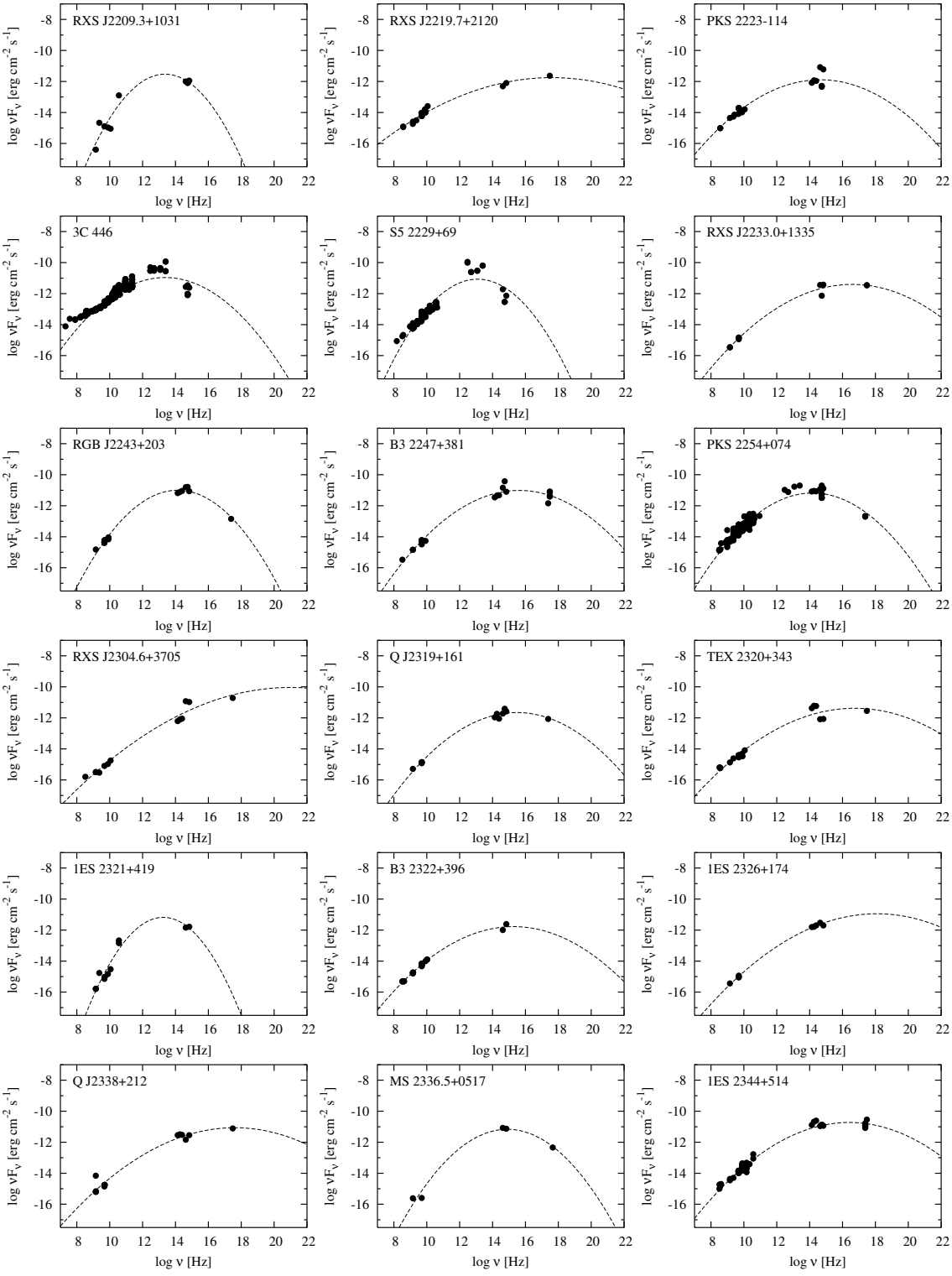

Fig. 13. continued.

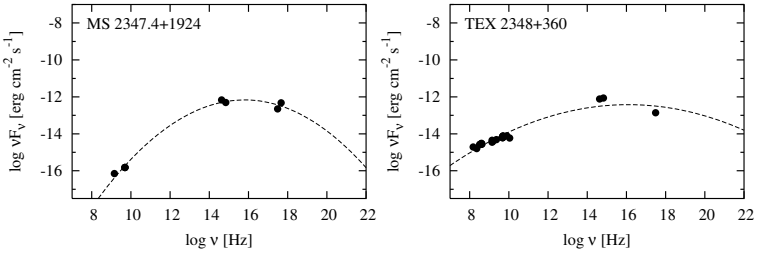

Fig. 13. continued.